

## Dynamic temporal evolution of polar cap tongue of ionization during magnetic storm

K. Hosokawa,<sup>1</sup> T. Tsugawa,<sup>2</sup> K. Shiokawa,<sup>3</sup> Y. Otsuka,<sup>3</sup> N. Nishitani,<sup>3</sup> T. Ogawa,<sup>2</sup> and M. R. Hairston<sup>4</sup>

Received 21 June 2010; revised 30 September 2010; accepted 6 October 2010; published 24 December 2010.

[1] During a magnetic storm on 14–16 December 2006, a polar cap tongue of ionization (TOI) was detected by an all-sky imager (ASI) at Resolute Bay, Canada (74.73°N, 265.07°E). We investigate the temporal evolution and spatial structure of the TOI in detail by combining the optical data with other observations (e.g., solar wind, GPS total electron content, SuperDARN, and DMSP and NOAA POES satellites). The TOI was observed as a bright and elongated 630 nm airglow plume for 4 h during the main phase of the storm. This interval corresponded to a period of prolonged stable large-amplitude southward IMF during a coronal mass ejection (CME). One to one and a half hours before the appearance of TOI, the polar cap boundary expanded rapidly far equatorward, and a positive ionospheric storm occurred. This implies that both the “expansion of the high-latitude plasma convection” and “build up of the source plasma in the midlatitudes” are necessary conditions for the formation of a TOI. Because both of them were triggered by a major southward turning of the IMF, the prolonged large-amplitude southward IMF orientation in the trailing part of the CME was primarily responsible for the generation of TOI. After its appearance, the TOI exhibited dynamic motion in the dawn to dusk direction. Simultaneous SuperDARN data suggest that a longitudinal progression of subauroral polarization stream controlled this dynamic motion. The optical TOI was found to be a continuous stream elongated in the noon-midnight direction although it contained some mesoscale patterns. Absence of large-scale temporal changes in the cusp plasma flow during the stable IMF period allowed the TOI to remain continuous without being broken into polar cap patches. The mesoscale structures within the TOI were probably produced by small-scale velocity fluctuations in the cusp plasma flow. The TOI as visualized with the all-sky airglow imager was found to be much more dynamic and much more complicated than we ever thought. The current study indicates that such a behavior of the TOI was presumably caused by a combination of temporal variations in the global-scale plasma circulation system, expansion and contraction of the polar cap area, and plasma density changes in the dayside low to midlatitudes.

**Citation:** Hosokawa, K., T. Tsugawa, K. Shiokawa, Y. Otsuka, N. Nishitani, T. Ogawa, and M. R. Hairston (2010), Dynamic temporal evolution of polar cap tongue of ionization during magnetic storm, *J. Geophys. Res.*, 115, A12333, doi:10.1029/2010JA015848.

### 1. Introduction

#### 1.1. Polar Cap Tongue of Ionization

[2] During magnetically disturbed conditions, solar-produced dense *F* region plasma can be transported by enhanced high-latitude convection electric fields from the daytime midlatitudes into the polar cap ionosphere through

the cusp inflow region. It has long been recognized that such a transport of high-density plasma would lead to the formation of a “tongue of ionization” (TOI) [Sato and Rourke, 1964]. A TOI is a discrete channel of enhanced *F* region plasma that extends from the daytime midlatitudes toward the nightside auroral region across the central polar cap. A TOI was first identified on a statistical basis from International Geophysical Year monthly median values of *F* region peak electron densities by Sato [1959]. Later, Knudsen [1974] revealed the contribution of rapid antisunward polar cap convection

<sup>1</sup>Department of Communication Engineering and Informatics, University of Electro-Communications, Tokyo, Japan.

<sup>2</sup>National Institute of Information and Communications Technology, Tokyo, Japan.

<sup>3</sup>Solar-Terrestrial Environment Laboratory, Nagoya University, Nagoya, Japan.

<sup>4</sup>William B. Hanson Center for Space Sciences, University of Texas at Dallas, Richardson, Texas, USA.

during periods of southward IMF for the formation of a TOI. More recently, *Moen et al.* [2008] statistically demonstrated that the diurnal variation in the  $F$  region peak density at around  $80^\circ$  magnetic latitude (MLAT) shows one maximum at around 12 MLT and another at around 23 MLT, implying convection-controlled transport of daytime plasma toward the nightside. These studies inferred that plasma transport associated with a TOI plays an important role in characterizing the plasma density distribution in the high-latitude ionosphere especially during southward IMF conditions.

[3] *Foster* [1984] statistically investigated incoherent scatter (IS) radar data from Chatanika in Alaska and showed that a region of enhanced plasma density matches the observed convection contours from lower latitudes in the postnoon sector toward the cusp and polar cap. Such a plasma transport feature during disturbed conditions has been observed also in individual cases [*Foster and Douppnik*, 1984; *Foster et al.*, 1985]. In particular, *Foster* [1989] clearly showed that a sunward convecting ionization feature extended along the equatorward edge of the postnoon midlatitude trough [*Moffet and Quegan*, 1983; *Rodger et al.*, 1992] and entered into the polar cap. This feature is now termed storm enhanced density (SED [*Foster*, 1993]); a latitudinally narrow stream of dense plasma forming at the equatorward edge of the duskside trough and extending toward the noontime cusp. *Foster et al.* [2007] demonstrated that such a plume of high-density plasma streaming poleward was carried by the low-latitude part of an enhanced convection at subauroral latitudes, called subauroral polarization stream (SAPS [*Foster and Vo*, 2002]).

[4] *Foster et al.* [2005] first visualized a complete 2-D structure of a transpolar TOI during a large magnetic storm on 20 November 2003, by using total electron content (TEC) data obtained from a large number of GPS receivers. It was well demonstrated that the daytime sunlit plasma was transported toward the nightside auroral region across the central polar cap as a large-scale plume. By compiling previous observational results, *Foster* [2008] claimed that the generation of transpolar TOI during a magnetic storm should be discussed in terms of the global-scale circulation of thermal plasma across a wide latitudinal area. In recent years, the tomographic inversion method based on the assimilation of global GPS data [see *Bust and Mitchell*, 2008, and references therein] has been employed to reconstruct the 2-D structure of polar cap TOIs [e.g., *Stolle et al.*, 2006; *Bust and Crowley*, 2007; *Yin et al.*, 2008; *Pokhotelov et al.*, 2008]. Since such a method is a very powerful tool for visualizing the large-scale electron density distribution, it is extensively used for investigating the global-scale plasma circulation associated with TOIs.

[5] TOIs are also known as a major source of polar cap patches; a polar cap patch is a chunk of increased plasma density whose spatial extent is of the order of a few hundred kilometers [e.g., *Crowley*, 1996]. Numerous processes have been proposed to explain the detachment of daytime dense plasma from a continuous TOI as discrete patches, such as the IMF-controlled reorientation of a cusp inflow region [*Decker et al.*, 1994; *Milan et al.*, 2002], convection jets [*Rodger et al.*, 1994], in situ plasma reduction under an intense electric field [*Valladares et al.*, 1994; *Ogawa et al.*, 2001], polar cap expansion and contraction [*Anderson et al.*, 1988], expansion of the polar cap convection pattern by pulsed reconnection

[*Lockwood and Carlson*, 1992; *Carlson et al.*, 2006], and bursty plasma transport from subauroral latitudes [*Moen et al.*, 2006]. Recent coordinated measurements of ionospheric plasma parameters around the dayside cusp have provided evidence for all of the above mentioned mechanisms, although it remains unclear which of these processes is the dominant one. An important point is that all the above mentioned processes commonly employ temporal variations of the plasma convection near the cusp to detach patches from a TOI; implying that the time varying plasma flow is an important factor for producing patches.

[6] Previous statistical analyses of IS radar data demonstrated that TOIs exist at least as an average feature even during only moderately disturbed conditions [*Foster*, 1984; *Moen et al.*, 2008]. However, the occurrence of a TOI, especially a transpolar large-scale TOI, appears to be very rare, whereas patches are observed much more frequently than TOI. Specifically, most of the large-scale TOIs were observed during large magnetic storms. For example, *Foster et al.* [2005] observed a transpolar TOI during a huge magnetic storm on 20 November 2003. This may indicate that, during moderately disturbed conditions (i.e., nonstormtime conditions), a TOI cannot extend deep into the central polar cap as a continuous channel because it is broken into patches soon after its entry into the polar cap by time varying plasma flow near the cusp. In order to confirm this hypothesis, we need to clarify the necessary conditions for keeping transpolar TOIs continuous and discuss why large-scale TOIs are often formed during large magnetic storms.

## 1.2. Optical Observation of TOI

[7] As mentioned in the previous part, the large-scale structure of SED/TOI plumes during magnetic storms has been extensively studied by *Foster* and colleagues mainly using GPS-TEC observations [*Foster*, 2008, and references therein]. Figure 1a shows an example of GPS-TEC observations of a transpolar TOI during the magnetic storm on 20 November 2003, which is adapted from *Foster et al.* [2005]. A huge stream of enhanced TEC traversing the central polar cap exists. This stream of high-density plasma originates from a region of elevated TEC in the postnoon midlatitudes. The superimposed convection streamlines derived from SuperDARN indicate that the channel of enhanced TEC is well aligned with the contours of the background plasma convection, suggesting that the daytime high-density plasma is first entrained into the noontime cusp as an SED, and then transported toward the nightside along the streamline of the polar cap convection as a transpolar TOI. This type of global TEC map is very useful for visualizing the large-scale structure of TOIs. However, we have not been able to discuss the rapid temporal evolution and/or small-scale spatial structure of TOI by using these TEC maps because their temporal and spatial resolutions are not always sufficient to resolve such variations.

[8] Figure 1b shows the optical signature of transpolar TOI during a magnetic storm on 15 December 2006, in the 630.0 nm airglow emission obtained from an all-sky airglow imager (ASI) operating in the northern part of Canada at Resolute Bay, which is adapted from *Hosokawa et al.* [2009c]. In the middle of the field-of-view (FOV), slightly duskward of the zenith of Resolute Bay, an unusually elongated bright airglow plume is seen; *Hosokawa et al.* [2009c]

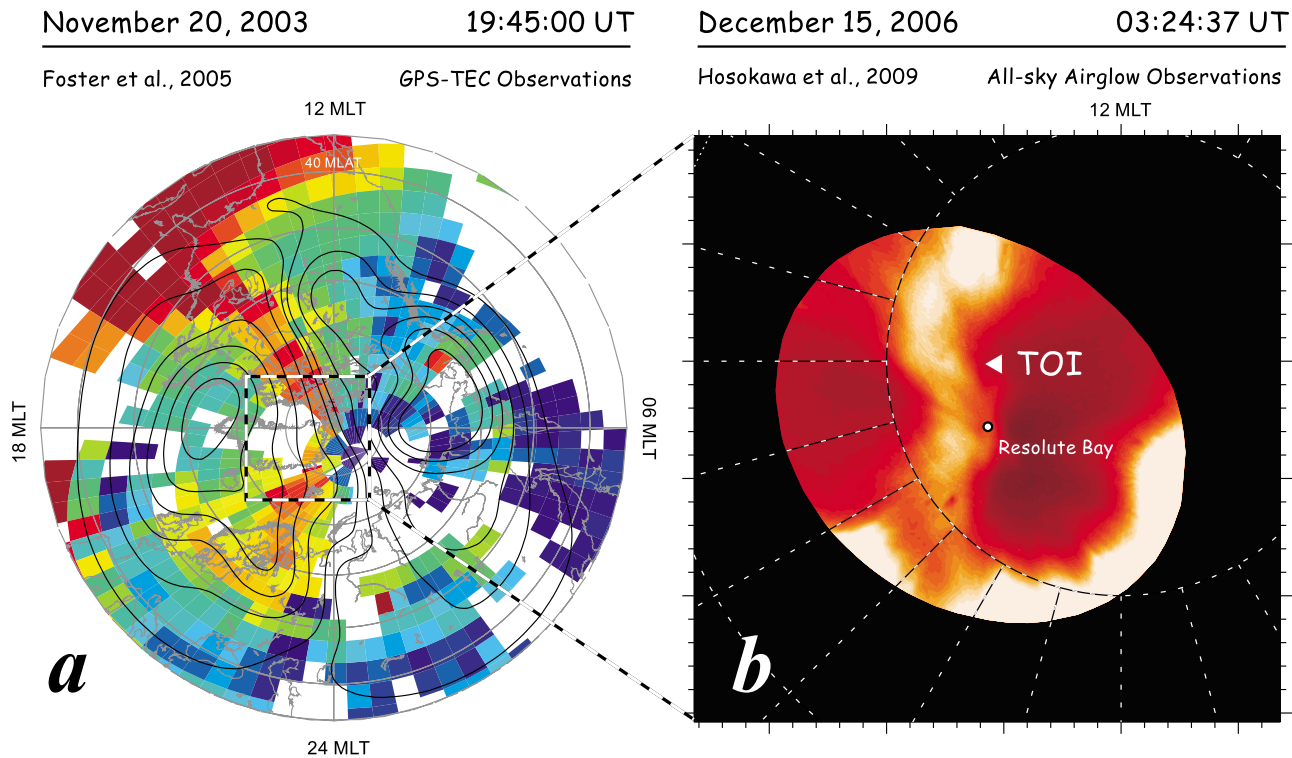


**Figure 1.** (a) First 2-D complete visualization of polar cap TOI by using GPS-TEC measurements during a magnetic storm on 20 November 2003. Adapted from *Foster et al.* [2005]. (b) Possible optical signature of polar cap TOI detected by an all-sky airglow imager at Resolute Bay, Canada, during a magnetic storm on 15 December 2006. Adapted from *Hosokawa et al.* [2009c].

interpreted this as an optical manifestation of a transpolar TOI by comparing this optical signature with the ion density data from a DMSP satellite. Although the FOV is confined only to the central polar cap near Resolute Bay, the ASI can capture 630.0 nm all-sky images with improved spatial resolution ( $256 \times 256$  pixels) every 2 min, allowing us to visualize the dynamic temporal evolution and small-scale spatial structure of the TOI in greater detail. In particular, the optical data well demonstrated that the TOI changed its position very dynamically possibly in association with the changes in the global-scale plasma circulation system. In this paper we use these optical data to clarify how the TOI develops during a magnetic storm from its start to end and compare its evolution with global data from other observations (e.g., GPS-TEC or SuperDARN), in order to address the following unclarified questions regarding the temporal evolution of TOI: “What triggered the TOI?” and “What controls the temporal evolution of the TOI?”.

[9] Another advantage of the ASI is its 2-D imaging capability that can be used to resolve possible smaller-scale structures within TOIs. As shown in Figure 1a, GPS-TEC maps cannot provide such a fine spatial resolution, especially in the central polar cap, because the number of the GPS receivers is obviously insufficient in the polar region. It has been known that plasma irregularities are often formed within patches [Tsunoda, 1988; Hosokawa et al., 2009a] and TOIs [Mitchell et al., 2005; De Franceschi et al., 2008]. These small-scale electron density perturbations impose significant scintillation on communication links from satellites along

their paths crossing the polar ionosphere. Thus, there is a strong requirement for modeling the satellite communication environment in the polar ionosphere to reveal the spatial distribution of patches and TOI in greater detail. Therefore, studies of the spatial structure of TOIs with improved resolution are important. By using all-sky optical data from Resolute Bay, *Hosokawa et al.* [2009c] succeeded in showing that the spatial structure of a TOI was far from uniform and it contained lots of small-scale structures embedded within its main body. Such fine-scale observations enable us to discuss “what process determines the spatial structure of TOI.”

### 1.3. Purpose of This Paper

[10] The study presented in this paper extends the work of *Hosokawa et al.* [2009c] by focusing on the temporal evolution of the transpolar TOI during the magnetic storm on 14–16 December 2006, using 2-D imaging observations from the ASI at Resolute Bay. We also use data from the SOHO and ACE spacecraft in the solar wind, low-Earth-orbiting (LEO) DMSP and NOAA POES spacecraft, SuperDARN, and GPS-TEC to conduct a multi-instrumental comprehensive analysis of a polar cap TOI during a large magnetic storm. In particular, we address the following questions regarding the temporal evolution of polar cap TOIs: “What dominates the appearance and disappearance of TOIs?” and “What controls the motion of TOIs?”. In addition, we discuss some unclarified issues regarding the spatial structure of TOIs by using the 2-D imaging capability of the ASI. The organization of this paper is as follows. In

section 2, we describe the data set used in this study. In section 3, observations of a transpolar TOI with the ASI and other instruments are presented. In section 4, we discuss the above mentioned outstanding issues regarding the temporal evolution and spatial structure of TOIs. Section 5 provides the conclusions of this paper.

## 2. Instruments

### 2.1. OMTIs All-Sky Airglow Imager at Resolute Bay

[11] The ASI employed in this study was developed by the Solar-Terrestrial Environment Laboratory, Nagoya University, as a part of the Optical Mesosphere Thermosphere Imagers (OMTIs) [Shiokawa *et al.*, 1999]. The OMTI system has been used to visualize a variety of ionospheric/thermospheric phenomena in the midlatitude and low-latitude regions, such as traveling ionospheric disturbances [Shiokawa *et al.*, 2003a, 2003b; Otsuka *et al.*, 2004a], plasma bubbles [Otsuka *et al.*, 2004b], and low-latitude aurora [Shiokawa *et al.*, 2005]. The imager at Resolute Bay (74.73°N, 265.07°E; AACGM latitude 82.9°) has been in operation since January 2005 as a part of the OMTIs [Hosokawa *et al.*, 2006]. This imager has a number of optical filters, such as 557.7 nm, 630.0 nm, 777.4 nm, Na-line, and OH-band; this enables us to study various upper atmospheric phenomena occurring in the polar cap region, such as polar cap patches [Hosokawa *et al.*, 2006, 2009a, 2009b, 2010], polar cap aurora [Koustov *et al.*, 2008; Jayachandran *et al.*, 2009], and gravity waves at mesospheric heights [Suzuki *et al.*, 2009a].

[12] The airglow intensity at a wavelength of 630.0 nm (OI 630.0 nm) obtained using a ground-based imager is known to be proportional to the electron density at 200–300 km altitudes in the *F* region [Barbier, 1959; Barbier and Glaume, 1962]. In this study, all-sky airglow images at a wavelength of 630.0 nm, which are obtained every 2 min with an exposure time of 30 s, are employed for visualizing the 2-D structure of the TOI in the polar cap region. Background continuum emission from the sky is sampled every 20 min at a wavelength of 572.5 nm and is used to derive the absolute intensity of the airglow lines [Shiokawa *et al.*, 2000, 2009]. The FOV of the ASI at 0200 UT on 15 December 2006, is indicated by the dashed circle in the MLT and AACGM magnetic latitude coordinates [Baker and Wing, 1989] in Figure 2. In this study, we assume that the altitude of the main optical emission was 250 km. In addition to the height assumption, a comparison of the all-sky images with star maps allows us to accurately determine the alignment of the camera. The FOV of the ASI shown in Figure 2 is mapped accordingly; it covers the duskside part of the central polar cap area during the interval of present study.

### 2.2. SuperDARN Radars

[13] The high-latitude convection maps presented in this study were derived from the coherent HF radars of Super Dual Auroral Radar Network (SuperDARN [Greenwald *et al.*, 1995; Chisham *et al.*, 2007]) in the Northern Hemisphere using the map-potential technique developed by Ruohoniemi and Baker [1998]. The radars of SuperDARN are capable of detecting backscatter from plasma irregularities at *F* region heights that are generated by plasma instabilities. Because these irregularities tend to drift at the background

plasma velocity, the line-of-sight component of ionospheric convection is measurable by examining the obtained Doppler spectra. During the interval described in this paper, the radars were operating in the fast normal-scan mode. In the current version of this mode, the radar scans through 16 beams every minute, with an integration time of 3 s for each beam, and these are binned into 75 range gates (separation between the gates is 45 km). When we derived the convection maps, the data from 12 radars in the Northern Hemisphere are integrated in 2 min intervals; thus, the temporal resolution of the map is 2 min. The FOVs of the Northern Hemisphere SuperDARN radars are shown in Figure 2; these cover a vast portion of the high-latitude ionosphere including the central polar cap area.

[14] In order to examine how the plasma drift in the equatorward portion of the high-latitude convection pattern contributes to the transportation of the midlatitude high-density plasma into the central polar cap area, we investigate the backscatter echoes from the midlatitude SuperDARN radar in Hokkaido, Japan (43.53°N, 143.61°E; AACGM latitude 36.46°;  $L = 1.546$ ). The recent deployment of the SuperDARN Hokkaido radar has enabled us to monitor storm-related high-speed subauroral flows [Ebihara *et al.*, 2008, 2009; Kataoka *et al.*, 2007] and some thermospheric waves [Ishida *et al.*, 2008; Ogawa *et al.*, 2009; Suzuki *et al.*, 2009b; Hayashi *et al.*, 2010]. As described in the latter part of this paper, the high-latitude convection pattern expanded equatorward considerably during the interval of this study. In such a situation, most SuperDARN radars in the auroral zone cannot observe the plasma drift near the cusp inflow region because such flows are located equatorward of the radar FOV. The SuperDARN Hokkaido radar is able to track the convection in the equatorward part of the convection pattern because it has a favorable viewing geometry. We also employ data obtained from the King Salmon SuperDARN radar in Alaska, which has a common viewing area with the Hokkaido radar, for tracking the temporal evolution of the plasma flow on the dayside.

### 2.3. GPS-TEC

[15] In this study, we employ GPS-TEC data to identify the signature of TOI or SED on the dayside. The GPS-TEC data are also used to observe the temporal evolution of the plasma distribution in the dayside low-latitude to midlatitude ionosphere, which could be a source of TOI/SED. The GPS data analyzed in this study were obtained via the FTP servers of the Continuously Operating Reference System (CORS), Scripps Orbit and Permanent Array Center (SOPAC), and International GNSS Service (IGS). There were about 2000 permanent GPS receivers available in December 2006. The distribution of the GPS receivers is overlaid in Figure 2 as blue dots. As shown in Figure 2, the density of the GPS receivers is obviously higher in the north American and European sectors. Almost all GPS receivers provide the data of the carrier phase and pseudorange measurements at two frequencies ( $f_1 = 1575.42$  MHz,  $f_2 = 1227.60$  MHz) every 30 s. The absolute TEC values were derived with a method based on Otsuka *et al.* [2002] in which a weighted least squares fitting is used to determine unknown instrumental biases, assuming that the hourly TEC average is uniform within the area covered by a GPS receiver. We neglect the TEC data from large satellite zenith angles (60–90°) to reduce cycle slips and errors due to conversion from slant to vertical

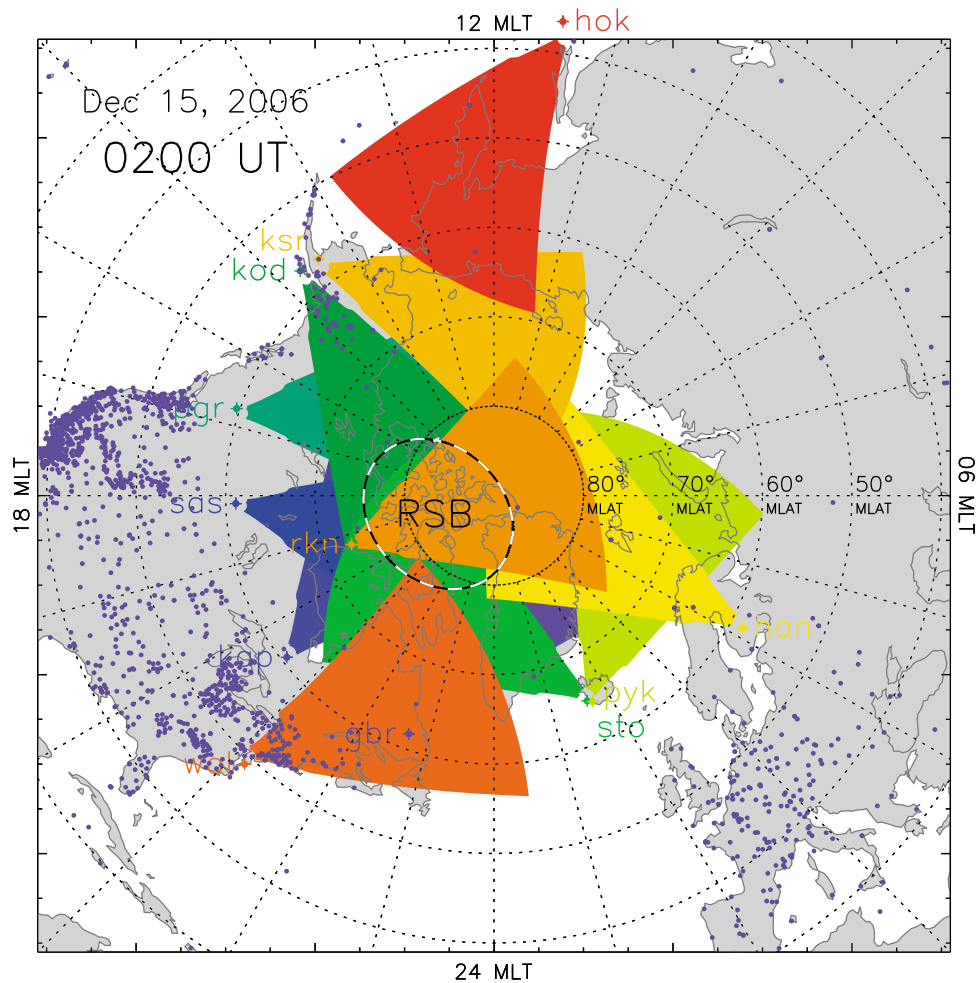


**Figure 2.** Location of the instruments at 0200 UT on 15 December 2006 in the MLT and AACGM magnetic latitude coordinates [Baker and Wing, 1989]. The magnetic noon is to the top, and dotted circles represent MLAT of 50°, 60°, 70°, and 80°. The FOV of the ASI at Resolute Bay is indicated by the dashed circle in the middle. The FOVs of the 12 SuperDARN radars in the Northern Hemisphere are shown as fan-shaped regions. The distribution of the GPS receivers is also overlaid as blue dots.

TEC. The TEC data shown in this paper have spatial resolution of  $1^\circ \times 1^\circ$  in latitude and longitude (with  $3 \times 3$  pixel smoothing) and temporal resolution of 30 s. These TEC data are mapped on the ionospheric height of 300 km.

#### 2.4. LEO Spacecraft: DMSP and NOAA POES

[16] We also use the ion density and cross-track ion drift data obtained by the SSIES instrument [Rich and Hairston, 1994] on board the DMSP satellites (DMSP F13, F15, F16, and F17) to identify the signature of TOI on the dayside part of the polar cap ionosphere. Because the altitude of the DMSP satellites is approximately 840 km, the signature of TOI in the DMSP ion density data is that in the topside ionosphere. In the latter part of this paper, we employ the auroral particle precipitation data from the SSJ/4 sensor [Hardy *et al.*, 1984] on board the DMSP satellites (DMSP F13, F15, and F16) and the TED instrument [Evans and Greer, 2000] on board the NOAA POES satellites (NOAA POES 15, 16, 17, 18, and METOP-02) to track the temporal evolution of the polar cap boundary. The SSJ/4 sensor on board DMSP mea-

sures downward fluxes of field-aligned (within  $3^\circ$  of vertical) ions and electrons from 30 eV to 30 keV in 19 channels, once per second. The TED instrument on board NOAA POES measures the directional energy flux carried toward the atmosphere by electrons and ions in the energy range from 50 eV to 20 keV. In particular, we use the data from sensors that view radially outward to observe the precipitating particles. The data of precipitating electrons and ions are provided as an integrated fluxes in two energy channels (50 eV to 1 keV and 1 keV to 20 keV).

### 3. Observations

#### 3.1. Overview of Storm on 14–15 December 2006

[17] In this paper, we present the temporal evolution of the polar cap TOI detected during an intense magnetic storm on 14–16 December 2006. This storm was led by a high-speed halo-type coronal mass ejection (CME) associated with the X3.4 flare at 0254 UT on 13 December 2006. Figure 3a shows the coronagraph difference image of the

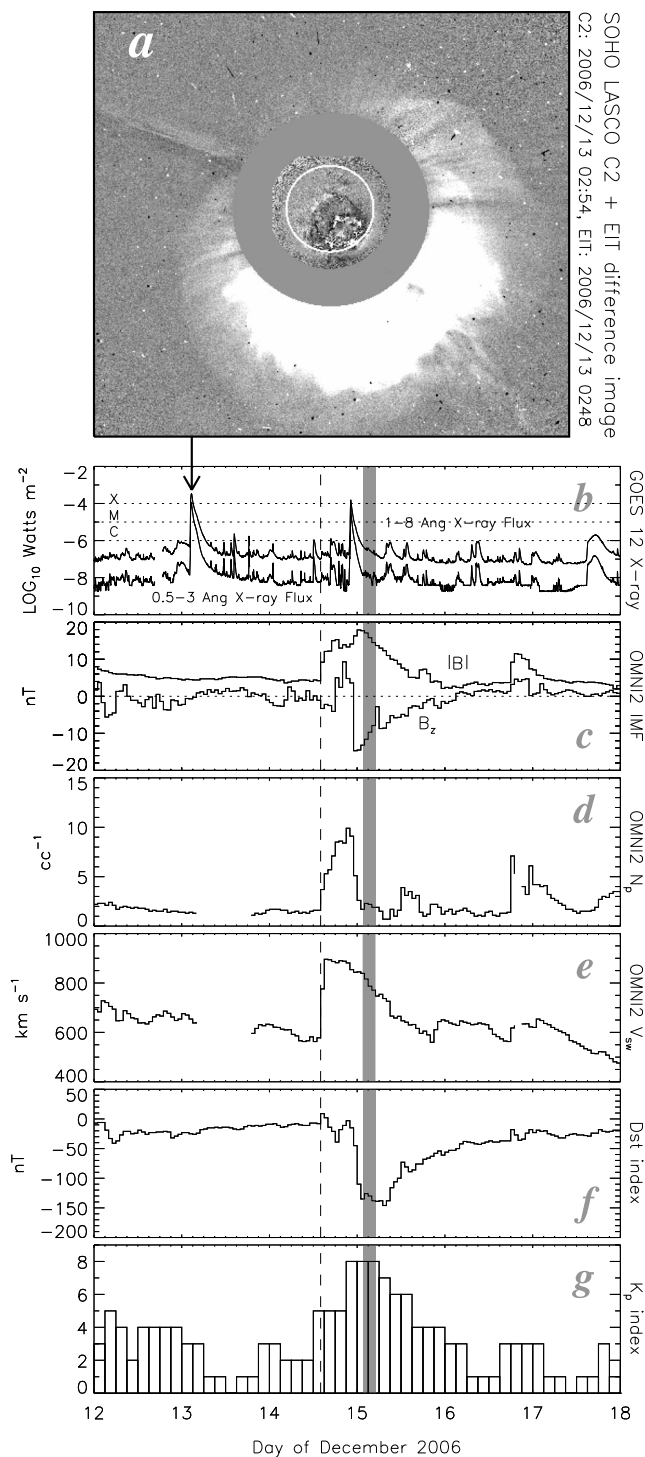


**Figure 3.** (a) Coronagraph difference images of the 13 December 2006 CME as seen by SOHO/LASCO C2. White circles indicate the position of the Sun. The images are adapted from the LASCO CME Catalog at NASA Goddard Space Flight Center. (b) X-ray fluxes in two wavelength bands obtained from the GOES 12 geosynchronous satellite during the week of this CME event. (c) Amplitude and  $z$  component of IMF, (d) solar wind number density, and (e) solar wind speed obtained from OMNI-2 database. (f)  $D_{st}$  index. (g)  $K_p$  index.

CME at 0254 UT on 13 December 2006, as seen by Solar and Heliospheric Observatory (SOHO)/Large Angle and Spectrometric Coronagraph (LASCO) C2. The eruption of the CME is clearly identified in the southwestern part of the image. The speed of the CME is estimated to be  $1774 \text{ km s}^{-1}$  ([http://cdaw.gsfc.nasa.gov/CME\\_list/](http://cdaw.gsfc.nasa.gov/CME_list/)). Figure 3b shows the X-ray fluxes in two wavelength bands obtained from the GOES 12 geosynchronous satellite during the week of this CME event. At the time of the flare, the X-ray flux clearly increased well above the level of an X-class flare. Figures 3c–3e show the OMNI-2 solar wind parameters obtained from the OMNI Web site (<http://omniweb.gsfc.nasa.gov/>). After the sudden arrival of an interplanetary shock at around 14 UT on 14 December 2006 (indicated by the vertical dashed line), we observed a typical signature of a magnetic cloud in the solar wind parameters (i.e., enhanced density and solar wind speed, enhanced IMF, and slow IMF rotation). A detailed discussion on the solar wind structure during this storm event was given by *Kataoka et al.* [2009]. The prolonged large-amplitude southward IMF in the trailing part of the magnetic cloud caused the large isolated CME-driven magnetic storm on 14–16 December 2006. The provisional  $D_{st}$  index (Figure 3f) reached  $-146 \text{ nT}$  at the storm peak. The  $K_p$  index shown in Figure 3g also increased to 8 during the initial and main phase of this storm. Almost 2 days after the launch of the CME, TOI was observed at Resolute Bay. The interval of the TOI is highlighted in grey in Figure 3. This interval corresponds to the main phase of this magnetic storm.

### 3.2. Solar Wind Structures

[18] As mentioned above, the magnetic storm was caused by a fast solar wind stream and a large southward component of the IMF in the trailing part of the magnetic cloud. In this part, we describe the solar wind structures during this storm in more detail. Figure 4 shows the IMF, solar wind parameters, AE index, and SYM-H index from 0400 UT on 14 December to 2000 UT on 15 December 2006. The shaded area denotes the period in which the optical signature of TOI was observed by the ASI at Resolute Bay. The IMF and solar wind parameters shown in Figure 4 were observed by the magnetometer (MAG [*Smith et al.*, 1998]) and solar wind electron, proton, and alpha monitor (SWEPAM [*McComas et al.*, 1998]) instruments on board the ACE spacecraft [*Chiu et al.*, 1998]. The spacecraft was located  $227\text{--}228 R_E$  upstream of Earth during this period. A shock occurred at 1350 UT (unshifted time) on 14 December at the ACE location; it can be identified by a sudden increase in the solar wind speed from  $600$  to  $900 \text{ km s}^{-1}$  (Figure 4e). The solar wind proton density also increased at this time (Figure 4f). After the shock, the solar wind speed decreased gradually, and it became approximately  $800 \text{ km s}^{-1}$  during the interval when the TOI was observed at Resolute Bay. This solar wind speed of approximately  $800 \text{ km s}^{-1}$  corresponds to a delay of 28 min between the observed IMF and solar wind features at ACE and its incidence on the dayside magnetopause. An additional 2 min are added to account for the propagation of Alfvén waves from the subsolar magnetopause to the dayside polar cap ionosphere. These calculations were carried out by the technique proposed by *Khan and Cowley* [1999]. The time series of the solar wind and IMF data shown in Figure 4 are shifted accordingly.

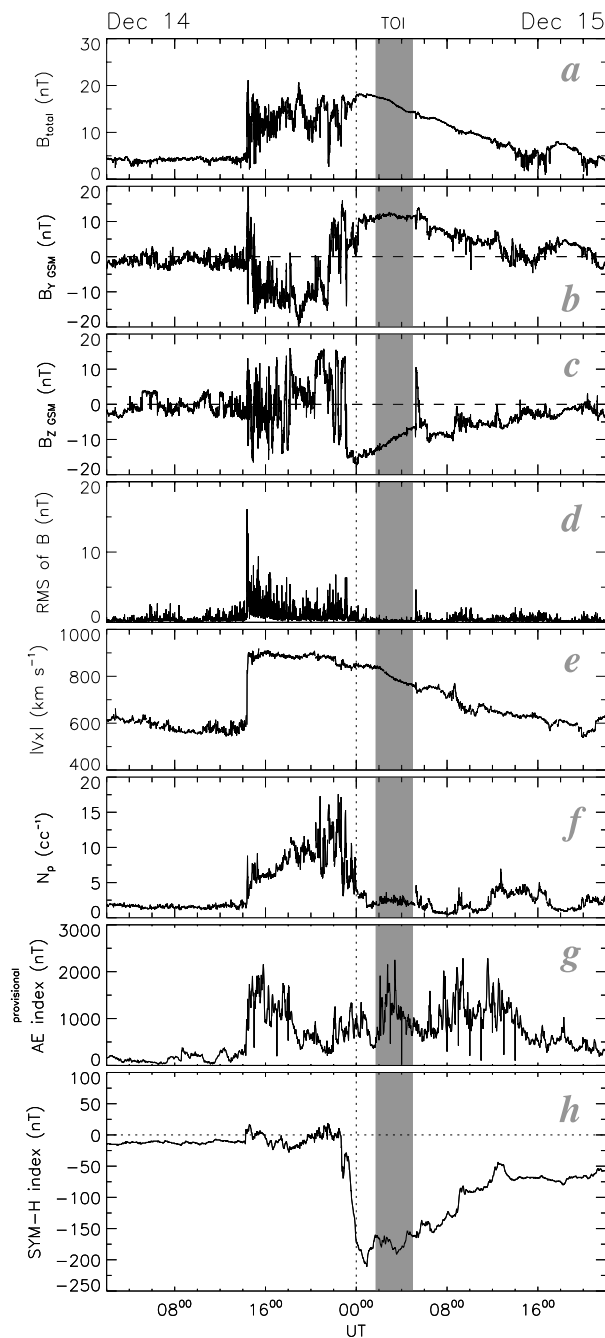


**Figure 4.** (a–f) Solar wind and interplanetary magnetic field conditions measured by the SWEPAM and MAG instruments on board the ACE spacecraft time shifted to the dayside magnetopause. (g) Provisional AE index. (h) SYM index H-component. Shaded area denotes the period in which the optical signature of TOI was observed by the ASI at Resolute Bay.

[19] The magnetic storm was initiated by a storm sudden commencement (SC) [Araki, 1994] at 1414 UT on 14 December, as seen in the SYM-H index (Figure 4h), that is almost equivalent to the 1 min  $D_{st}$  index [Iyemori and Rao, 1996]. The accuracy of the time lag of 30 min estimated above is confirmed by the correspondence between a sharp increase in the solar wind speed and the SC. The

SYM-H started decreasing significantly at around 2240 UT on 14 December (approximately 8 h after the SC) and reached its minimum value ( $-211$  nT) at around 0100 UT on 15 December. Our interval of interest, 0140–0500 UT on 15 December (highlighted in grey in Figure 4), corresponds to the main phase of this magnetic storm, during which the polar cap TOI was observed by the ASI at Resolute Bay. The provisional AE index, as shown in Figure 4g, indicates that auroral activity also commenced soon after the arrival of the shock and continued throughout this storm interval.

[20] During the interval of TOI (0140 to 0500 UT on 15 December 2006), the  $B_y$  component of IMF was stable at around 10 nT (Figure 4b) and  $B_z$  changed very gradually from  $-14$  to  $-7$  nT (Figure 4c), which is a typical signature of magnetic cloud embedded in CME [e.g., Burlaga et al., 2001; Kataoka and Miyoshi, 2006]. Such a prolonged large-amplitude southward IMF in the trailing part of the magnetic cloud could contribute to the formation of the TOI in the central polar cap area. Another important point to note is that the temporal variability of the IMF during the TOI event was quite different from that in the initial phase of this magnetic storm. The three IMF parameters shown in Figures 4a–4c indicate intense magnetic field fluctuations throughout the initial part of this solar wind disturbance (1414–2300 UT on 14 December). In particular, the  $B_z$  component of IMF started oscillating soon after the arrival of the shock, and such an oscillation continued until the end of the initial phase at around 2300 UT. During this interval of intense IMF fluctuation, the solar wind proton density was largely enhanced (Figure 4f), indicating that the compressed solar wind structure downstream of the shock caused the fluctuation in the IMF [e.g., Kataoka et al., 2005]. At 2300 UT on 14 December, the  $B_z$  component of IMF exhibited rapid southward turning, leading to the beginning of the main phase of this storm. Soon after the start of the main phase, the solar wind proton density decreased to 2–3 nPa and fluctuations in the IMF ceased. The disappearance of the rapid IMF fluctuation can be more clearly seen in the root mean square (RMS) of the total magnetic field shown in Figure 4d. An important point to remind is that the fluctuation level was quite low in the later stage of the main phase, when the TOI was observed at the polar cap region. We discuss the possible relationship between the formation of a TOI and the disappearance of IMF fluctuations in section 4.

### 3.3. Bright Optical Plume at Resolute Bay: Optical Signature of TOI?

[21] Figure 5 shows a time sequence of 630.0 nm airglow images picked at 10 min intervals from 0130 to 0520 UT on 15 December 2006. The original all-sky images have been converted into altitude adjusted corrected geomagnetic (AACGM) coordinates [Baker and Wing, 1989] assuming an emission height of 250 km and then mapped into MLAT/MLT coordinates. The magnetic midnight is to the bottom and dotted circles represent MLAT of  $70^\circ$  and  $80^\circ$ . Here the absolute optical intensities are color scaled in units of Rayleigh. It should be noted that the prominent feature near the equatorward part of the FOV (for example, Figures 5i–5t) corresponds to the poleward part of the main auroral oval. The AE index plotted in Figure 4g suggests that a number of substorms occurred during this magnetic storm. In particular, an intense substorm (AE index  $\approx 2000$  nT)

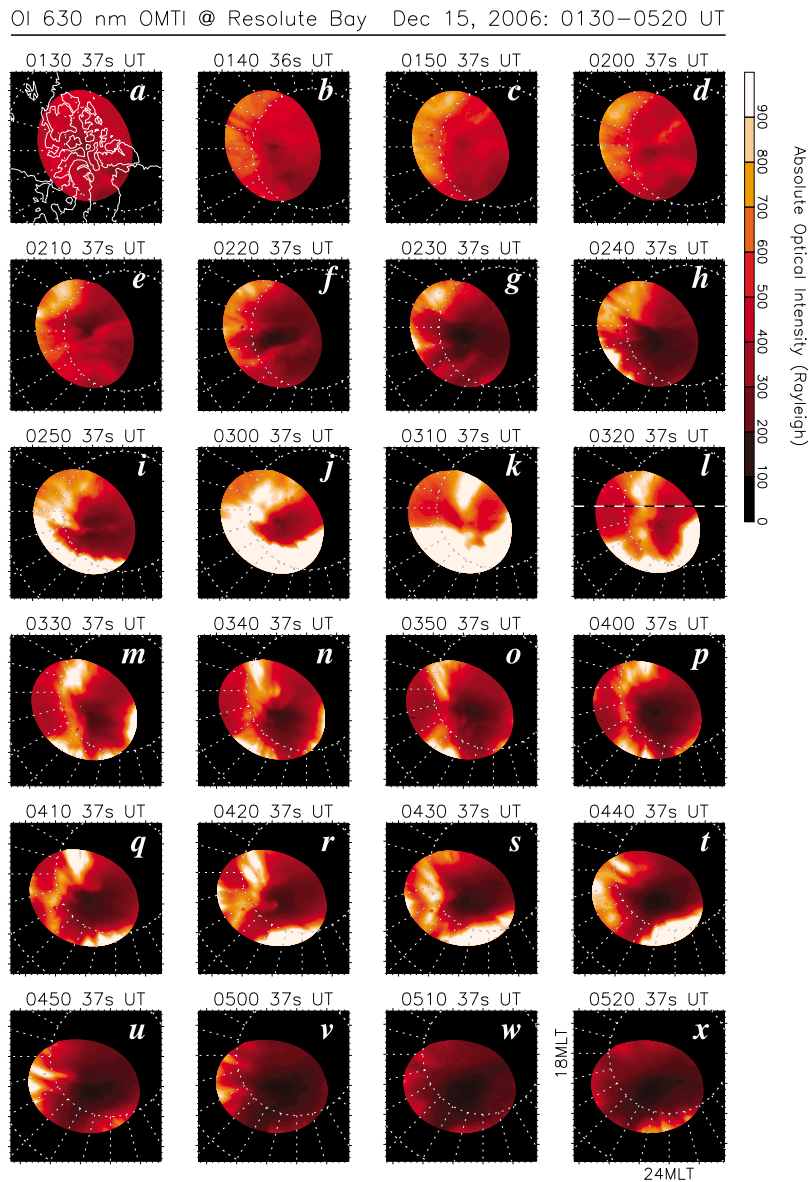


**Figure 5.** (a–x) Sequence of 630.0 nm airglow images at 10 min intervals from 0130–0520 UT. The original all-sky images have been converted into AACGM coordinates assuming an emission height of 250 km and then mapped into MLAT/MLT coordinates. The magnetic midnight is to the bottom and dotted circles represent MLAT of 70° and 80°. Here the absolute optical intensities are color scaled in units of Rayleigh.

occurred during the interval shown in Figure 5. Thus, the equatorward part of the FOV was occasionally illuminated by the poleward expanding aurora during the expansion phase of the substorm.

[22] At 0140 UT (Figure 5b), a bright airglow plume first appeared near the duskside edge of the FOV and this structure stayed below 80° MLAT for approximately 1 h. At 0130 UT (Figure 5a), no clear signature of the plume was identified at least within the FOV of the ASI. At around 0250 UT (Figure 5i), the plume started moving poleward and then reached the central part of the FOV at 0320 UT (Figure 5l). The image at 0320 UT is the highlight of this interval because the spatial structure of the plume was most clearly identified as a continuous channel of enhanced

luminosity elongated along the noon-midnight line. This elongation in the noon-midnight direction implies that the plume was composed of high-density plasma transported from the dayside sunlit area as a transpolar TOI. After 0320 UT, the plume remained almost stable for approximately 1 h although it changed its spatial structure dynamically. After 0500 UT, the plume moved almost off the FOV because the FOV shifted toward midnight according to Earth's rotation.

[23] In order to better demonstrate the dynamic behavior of the plume, an animation showing its temporal evolution can be found in the auxiliary material.<sup>1</sup> In the left-hand

<sup>1</sup>Auxiliary materials are available in the HTML. doi:10.1029/2010JA015848.

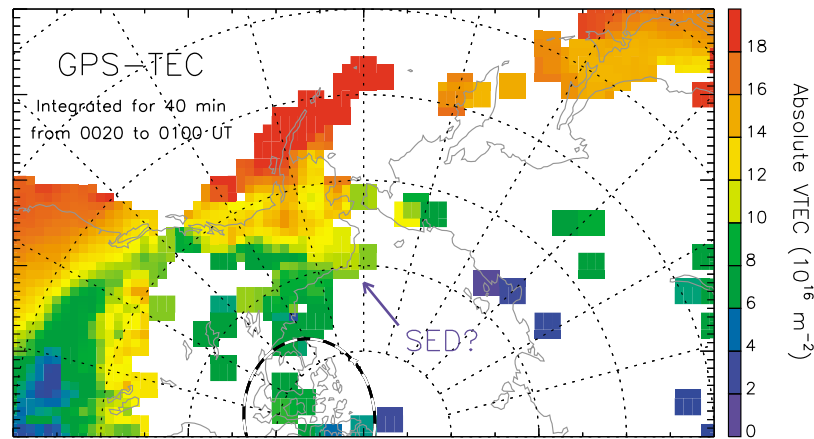


**Figure 6.** GPS-TEC map at 0040 UT on 15 December which is approximately 1 h before the appearance of the optical plume at Resolute Bay. The FOV of the ASI at Resolute Bay is indicated by the dashed circle in the bottom. To create this map, the original GPS-TEC data obtained every 30 s are integrated for 40 min from 0020 to 0100 UT to increase the number of data points. Possible indication of SED penetrating from the midlatitude into the cusp inflow region is indicated by the blue arrow.

frame of the animation, 630.0 nm airglow images are shown at a rate of one frame every 2 min in the same format as that in Figure 5. The animation clearly shows that some meso-scale patterns were embedded within the main body of the plume and these drifted antisunward. This directly indicates that the plasma within the plume was transported antisunward from the dayside toward the nightside across the polar cap, possibly along the streamline of the plasma convection, suggesting that the source of the plume was located on the dayside. In the right-hand frame of the animation, the optical images are plotted together with the GPS-TEC measurements and the SuperDARN map potential contours; this should be useful in determining how the ionospheric plasma distributed and circulated on a global scale.

[24] The elongation of the plume in the noon-midnight direction implies that the plume was composed of high-density plasma transported from the dayside sunlit area as a transpolar TOI. However, the FOV of the ASI is too narrow to observe the entire structure of the plume; thus, we cannot definitely determine if the plume actually extended from the dayside continuously. In particular, from only the optical data, it remains unclear how the high-density plasma was entrained into the polar cap near the dayside cusp. In order to clarify this issue, we tried to find a signature of transpolar TOI in the GPS-TEC data during the interval of the optical plume. Figure 6 shows the GPS-TEC map at 0040 UT on 15 December, which is approximately 1 h before the appearance of the optical plume at Resolute Bay. To create this map, the original GPS-TEC data obtained every 30 s were integrated for 40 min from 0020 to 0100 UT to increase the number of data points. At this time, there were some GPS receivers in Alaska and the Aleutian Islands covering the postnoon part of the dayside ionosphere. Thus, it is well identified that solar produced high-density plasma ( $>15$  TECU) was distributed below  $60^\circ$  MLAT, which could be the source of the TOI seen in the central polar cap. However, North America, where a number of GPS receivers are available, was located on the duskside during the interval of the TOI plume (from 0140 to 0500 UT); we could not

identify how the dense daytime source plasma was entrained into the polar cap as a TOI. Nonetheless, there is some indication of a SED [Foster, 1993] penetrating from the midlatitude into the cusp inflow region, as indicated by the blue arrow in Figure 6. This signature seems to originate from the equatorward part of the midlatitude trough that is seen as a region of decreased TEC on the duskside [Rodger *et al.*, 1992]. Hence, the high-density midlatitude plasma was actually transported at least toward the cusp inflow region as an SED. However, the number of GPS receivers is insufficient to discuss the relationship between the signature of the SED and the optical plume over Resolute Bay. Hence, it still remains uncertain whether the optical plume actually extended from the dayside source region toward the central polar cap continuously.

[25] Because the signature of the optical plume cannot be clearly seen in the GPS-TEC data, we intend to clarify how the plume extended from the dayside by using the ion density data from the DMSP spacecraft and the plasma convection measurement from SuperDARN. Figure 7a shows the ASI image at 0410 UT in which the optical plume was seen in the duskside part of the FOV as an elongated bright stream. Around this time, DMSP F13 passed through the dayside part of the polar cap, whose track is superimposed on Figure 7a. Figure 7c shows the ion density data at 860 km altitude from DMSP F13 along the track. The ion density increased from  $10^{10}$  to  $10^{11}$   $\text{m}^{-3}$  at 0408:10s UT and decreased at around 0411:30 s UT. This interval of elevated ion density is marked by a horizontal red line on the top of Figure 7c and in Figure 7a (from B to C at around  $75^\circ$  MLAT on the dayside). Foster *et al.* [2005] used incoherent scatter radar observations to show that a TOI can be observed even at altitudes higher than 800 km. This implies that a TOI is not thin in altitude but extends from the lower  $F$  region to the topside ionosphere. Thus, the region of enhanced ion density shown in Figure 7c is considered to be the dayside part of the optical plume over Resolute Bay.

[26] We also overlay the contours of electric potential derived from SuperDARN in Figure 7a, from which we

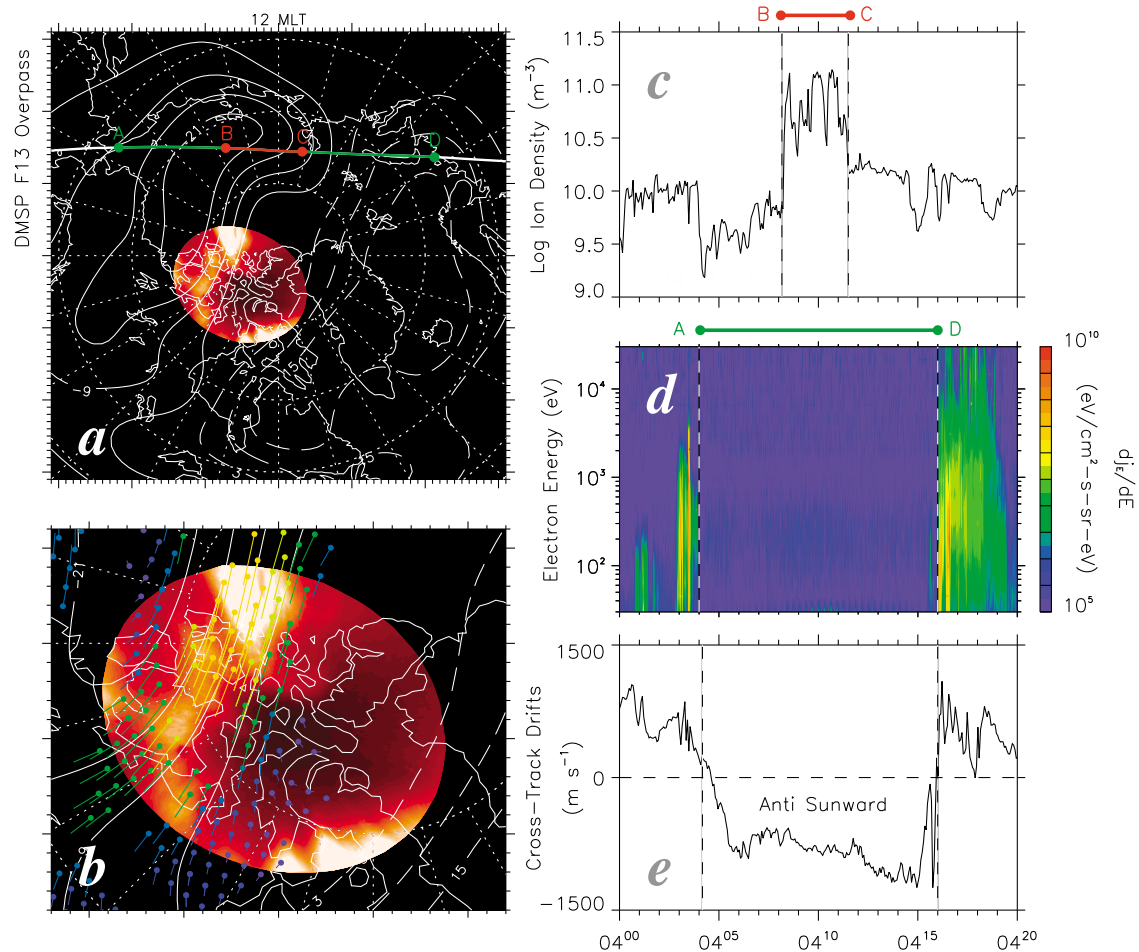


**Figure 7.** (a) A 630.0 nm airglow image at 0410 UT, in which the contours of electric potential derived from SuperDARN are overlaid. Superimposed thick line is the track of the overpassing DMSP F13 satellite. (b) A 630.0 nm airglow image at 0410 UT, in which the contours of electric potential and velocity vectors derived from SuperDARN are overplotted. (c–e) Ion density, precipitating electrons, and cross-track ion drift measurements from the overpassing DMSP F13 satellite.

roughly trace the streamline of the polar cap convection. It is clearly seen that the region of ion density enhancement detected using DMSP and the optical plume over Resolute Bay were situated in the same convection streamline. In Figure 7b, we again plot the ASI image at 0410 UT together with the vectors and contours of the SuperDARN map potential data. The trajectory of the plume was collocated with the antisunward stream of the polar cap convection. This reconfirms that the plasma within the plume was transported from the source on the dayside along the polar cap convection. A comparison of the optical plume with the ion density enhancement and convection streamline suggests that the plume observed over Resolute Bay was not a local structure but a large-scale feature extending continuously from the dayside into the central polar cap. Hence, the bright optical plume seen by the ASI at Resolute Bay was indeed an optical signature of a transpolar TOI.

[27] A comparison of the data from ASI, DMSP and SuperDARN strongly suggests that the plume seen over Resolute Bay was actually an optical manifestation of a transpolar TOI. In addition, the DMSP data imply that the

source of the plume is located at least some degree equatorward of the ion density enhanced region located at around 75° MLAT. In general, the dense plasma within a TOI is considered to be captured and transported from midlatitudes by the high-latitude convection. Thus, it is important to determine how the polar cap boundary (PCB) expanded at this time. Figure 7d shows energy spectrogram of electrons from DMSP F13. Marked enhancements of electron energy flux are identified before 0404 UT and after 0416 UT, corresponding to the electron auroral oval in the dusk and dawn sectors, respectively. In the region sandwiched by these precipitations, there exists a region of no auroral particle precipitation. The cross-track ion drift measurement along the DMSP track shown in Figure 7e demonstrates that the convection was directed antisunward in this region. These data suggest that this region without particle precipitation (from A to D) corresponds to the polar cap. The equatorward boundary of the polar cap along the DMSP track is located at approximately 63° MLAT, that is 10–15° lower than its nominal position. Thus, the PCB expanded equatorward extremely at least at around 0410 UT. Such an expansion of

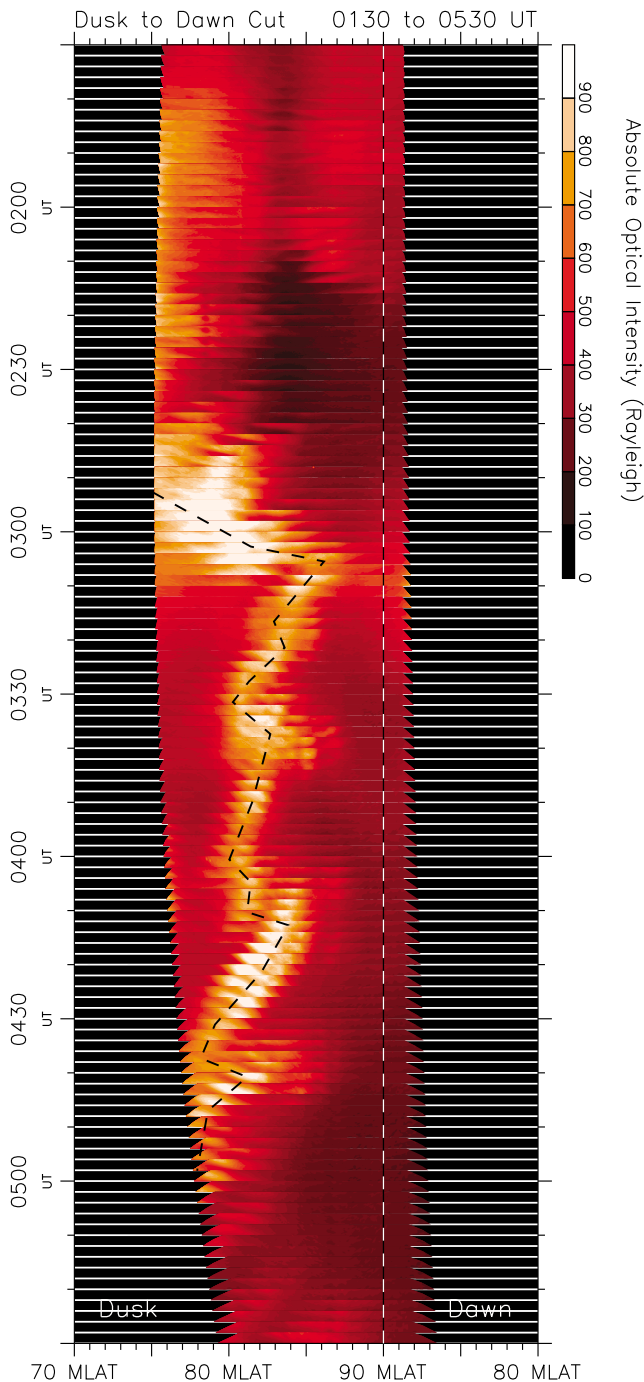


**Figure 8.** A keogram reproduced from the 630.0 nm all-sky images from dawn to dusk (i.e., 18 MLT to 06 MLT) cross section as indicated by the dashed line in Figure 5I. The vertical axis is UT from 0130 to 0530 UT and the horizontal axis is the MLAT from 70° on the duskside to 80° on the dawnside across the magnetic pole, which is indicated by the vertical dashed line. The trajectory of the plume after the major downward excursion at around 0250 UT is traced by the dashed line.

the PCB could greatly contribute to the transportation of the midlatitude dense plasma into the dark polar cap ionosphere. In section 4, we examine how the polar cap extent changed during this storm event and discuss the relationship between the appearance of the transpolar TOI plume and the polar cap expansion.

### 3.4. Temporal Evolution of TOI

[28] The primary objective of this study is to clarify the dynamic evolution of the polar cap TOI by using all-sky optical images obtained every 2 min over Resolute Bay. In particular, we intend to discuss what triggered the TOI and what controlled its temporal evolution. To gain a better understanding of the temporal evolution of the TOI, Figure 8 shows a keogram reproduced from the 630.0 nm all-sky images from dawn to dusk (i.e., 18 MLT to 06 MLT) cross section as indicated by the dashed line in Figure 5I. The vertical axis is UT from 0130 to 0530 UT and the horizontal axis is the MLAT from 70° on the duskside to 80° on the dawnside across the magnetic pole, which is indicated by the vertical dashed line. The TOI plume first appeared at around 0140 UT near the duskside edge of the FOV. After its appearance, the TOI stayed below 80° MLAT for approximately 1 h until 0250 UT. Then, the plume suddenly started moving downward (i.e., poleward) and reached the zenith of Resolute Bay at 0305 UT. During this excursion, the TOI moved downward for approximately 1000 km in around 15 min; thus, the speed of the downward excursion was as high as  $1 \text{ km s}^{-1}$ . The trajectory of the plume after the major downward excursion at around 0250 UT is traced by the dashed curve in the keogram to better show its dynamic temporal evolution. After the TOI arrived at the zenith of Resolute Bay, the plume gradually changed its location toward dusk whereas the plume occasionally exhibited short downward excursions in MLAT, again demonstrating that the TOI plume as seen by the ASI is much more dynamic than that visualized in the GPS-TEC maps. Finally, the plume moved out of the FOV at around 0500 UT. This disappearance of the plume was associated with both the shift of the FOV according to Earth's rotation and gradual duskward motion of the plume itself.

[29] As mentioned above, the TOI appeared within the FOV of the ASI at around 0140 UT. However, this does not always correspond to the onset of the TOI because the ASI was observing a limited viewing area within the entire polar cap. Here, we employ the ion density data from DMSP passing through the dayside part of the polar cap and try to identify the onset time of the TOI more exactly. In Figures 9a–9g, the ion density data from DMSP are color coded along their orbits for seven intervals from 2000 UT on 14 December to 0900 UT on 15 December. The optical data from Resolute Bay are superimposed on the map only when the optical signature of TOI was identified (Figures 5c–5f). Figures 5h–5n show the ion density data from one of the DMSP orbits plotted in Figures 5a–5g. The time when the spacecraft passed through the noon meridian is indicated to aid the discussion. In Figure 9a, the ion density data from DMSP well before the appearance of the TOI (from 2000 UT on 14 December to 0030 UT on 15 December) are shown. Any discrete enhancement of the ion density cannot be seen in the polar cap area along all DMSP orbits. The ion density data from DMSP F13 plotted in Figure 9h also reveal an absence of

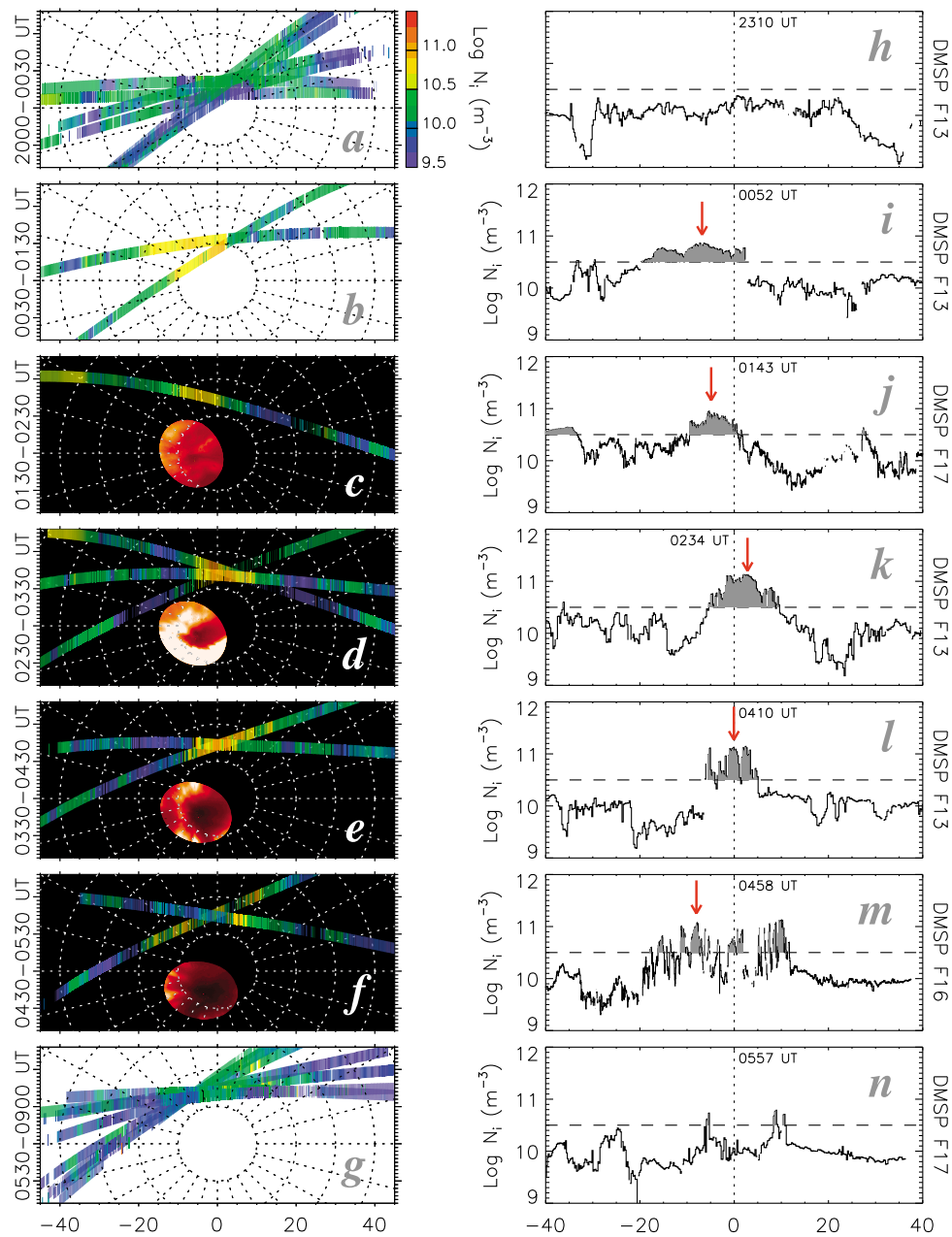


**Figure 9.** (a–g) The ion density data from DMSP color coded along their orbits. The optical data from Resolute Bay are superimposed on the map only when the optical signature of TOI was identified. (h–n) The ion density data from one of the DMSP orbits plotted in Figures 9a–9g, in which the time when the spacecraft passed through the noon meridian is indicated to aid the discussion. The ion density enhancement associated with TOI is indicated by the red arrow.

ion density enhancement associated with the TOI, suggesting that the TOI had not appeared at least before 0030 UT on 15 December.

[30] In the next period (Figures 5b and 5i, from 0030 to 0130 UT on 15 December), the optical data are not shown because the TOI had not yet appeared within the FOV. However, the DMSP data reveal that the ion density was enhanced up to  $10^{11} \text{ m}^{-3}$  on the duskside part of the dayside polar cap. The ion density data from DMSP F13 shown in Figure 9i more clearly indicate that the ion density was

enhanced in the polar cap, as indicated by the red arrow. This suggests that the TOI had appeared at least before around 0050 UT on 15 December. From 0130 to 0430 UT (Figures 9c, 9j, 9d, 9k, 9e, and 9l), both ASI and DMSP observed a signature of TOI as an increase in the airglow intensity and ion density, respectively. The location of the region of enhanced ion density agrees well with the structure of the optical plume although there is a small gap between the orbit of DMSP and the FOV of the ASI. That is, both instruments detected a part of the large-scale structure of

TOI extending for a long distance from the dayside deep into the central polar cap. From 0430 to 0530 UT (Figures 9f and 9m), the distribution of the enhanced ion density region became patchy, which is more clearly seen in Figure 9m. This indicates that the TOI had started to show spatial substructures within it at around 0500 UT. A combination of the data from DMSP and ASI shows that the TOI had appeared at least before 0050 UT on 15 December and continued for at least 4 h until around 0500 UT. Another important point to note is that the location of the region of enhanced ion density shifted downward at around 0230 UT as shown in Figure 9k, which is consistent with the major downward excursion of the optical plume shown in Figure 8.

### 3.5. Spatial Structure of TOI

[31] Another important objective of this paper is to reveal the spatial structure of transpolar TOI by utilizing the two-dimensional imaging capability of the ASI. The complete 2-D mapping of TOI has already been carried out by using global GPS-TEC measurements [Foster *et al.*, 2005]. However, the spatial and temporal resolution of their GPS-TEC map was not always sufficient to clarify the spatial structure of the TOI plume in greater detail. As mentioned in the previous part, the optical data clearly indicate that the optical TOI was elongated in the noon-midnight direction as a very narrow and continuous stream. In addition, the improved spatial and temporal resolution of the ASI allows us to find some mesoscale structures (patterns) embedded within the main body of the plume. Here, we summarize the important characteristics of the optical signature of the TOI with regard to its spatial structure. In addition, we indicate some differences between polar cap patches and TOIs in terms of their optical intensity and/or spatial structure for discussions in the latter part of this paper.

[32] The keogram shown in Figure 8 indicates that the width of the TOI plume along dusk to dawn cross section varied slightly with time; however it was generally  $3^{\circ}$ – $5^{\circ}$  in MLAT, corresponding to a horizontal distance of 300–500 km. That is, the width of the TOI was considerably narrower compared to its extent in the direction of elongation (i.e., noon-midnight direction). The width of the region of enhanced ion density in the DMSP ion density data was also narrower compared to the entire polar cap extent (Figure 7). These observational facts may suggest that the background antisunward convection increased only within the narrow area of the plume; then, the plume was delivered by a narrow channel of extremely rapid antisunward convection extending from the dayside cusp deep into the polar cap. However, the cross-track ion drift measurement along the DMSP track (Figure 7e) indicates no particular enhancement of the speed of the antisunward convection within the TOI. This implies that there existed another factor controlling the width of the plume.

[33] Foster *et al.* [2005] found that the TEC within a TOI was greatly elevated, suggesting that the source of the TOI is midlatitude plasma transported from the dayside [Foster, 1993]. The current observation also indicates that the optical intensity within the optical TOI was as large as 500 R, which is 3–5 times brighter than that of polar cap patches. This indicates that the plume observed over Resolute Bay was also of a lower-latitude origin. Another important feature is that the spatial structure of the plume was far from

uniform. As mentioned briefly in the previous part, Figure 5 shows that some mesoscale structures existed within the plume, although the main body of the plume was elongated continuously at least within the FOV of the ASI. These smaller-scale patterns were drifting antisunward along the structure of the plume; this may be better viewed in the animation in the auxiliary material. Hosokawa *et al.* [2009c] estimated the typical horizontal extent of these mesoscale features to be 250–600 km. These values are very similar to the spatial-scale size of polar cap patches [Coley and Heelis, 1995]. We discuss the process that produces these patterns within the TOI in section 4.

[34] The current optical observation of TOI suggests that the TOI was quite different from patches in terms of its luminosity and spatial structure. Figure 10 summarizes the differences between patches and a TOI. Figures 10a and 10b show typical examples of polar patches and a TOI. Figures 10c and 10d show schematic illustrations of polar patches and TOI. Polar cap patches are normally observed as individual regions of airglow enhancement, as shown in Figure 10a. They are mostly observed as a circular or cigar-shaped discrete structure that is elongated somewhat in the dawn-dusk direction [MacDougall and Jayachandran, 2007]. In contrast, the TOI plume observed during the current interval was more continuous in the noon-midnight direction, although there existed some mesoscale structure embedded within its main body. In addition, the TOI plume was clearly narrower in the dawn-dusk direction, as shown in Figure 10b. Obviously, there exist significant differences between the optical plume and patches that are more frequently observed during nonstormtime periods. We discuss why the spatial structure of TOI significantly differs from that of patches in section 4 and try to clarify the process that produces such differences.

## 4. Discussion

### 4.1. What Triggered the TOI?

[35] As described in section 3.4, the TOI appeared at the polar cap latitude at some stage between 0030 UT and 0050 UT on 15 December and continued for approximately 4 h. First, we discuss what controlled the appearance and disappearance of the TOI. Here, we divide the generation of TOI into two processes, “transportation of the source plasma into the central polar cap” and “setup of the high-density source plasma in midlatitudes,” and discuss these processes separately.

[36] Figure 11 schematically illustrates the winter-time high-latitude plasma environment during quiet or moderately disturbed (Figure 11a) and storm conditions (Figure 11b). In the situation shown in Figure 11a, the high-latitude plasma convection system is located within the dark hemisphere; thus, it cannot interact with the dense plasma distributed equatorward of the terminator. This does not allow the plasma convection to transport the dense daytime plasma into the polar cap area as a TOI. In contrast, during storm time, as shown in Figure 11b, the PCB extends into the sunlit area and the antisunward convection within the PCB interacts with the high-density plasma equatorward of the terminator. In such a situation, the high-latitude plasma convection system can entrain dense midlatitude plasma toward the central polar cap area through the cusp inflow region as a TOI. In reality, Figure 7 shows that the PCB was located at

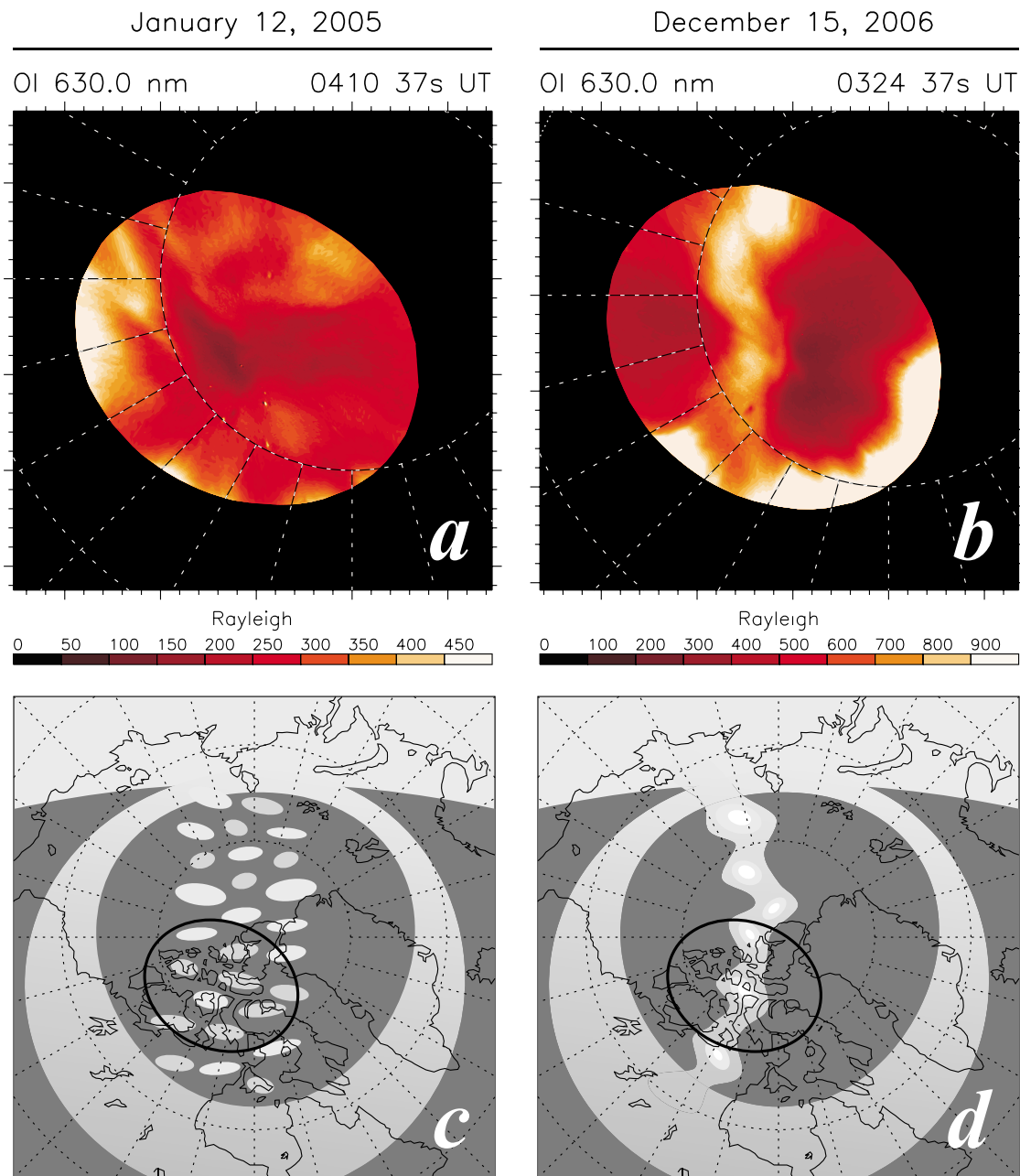


**Figure 10.** Typical examples of (a) polar cap patches and (b) TOI. Schematic illustrations of (c) polar cap patches and (d) TOI. The FOV of the ASI at Resolute Bay is indicated by the thick black circle in the middle of Figures 10c and 10d.

approximately  $65^\circ$  MLAT at 0410 UT on 15 December, i.e.,  $10\text{--}15^\circ$  lower than its nominal position. In addition, as the PCB expands equatorward, the convection outside the PCB (i.e., on closed field lines) extends further into the lower latitudes, allowing the flow on closed field lines to capture dense plasma of duskside or dawnside midlatitude origin. Foster *et al.* [2005] demonstrated that a TOI originated from a SED [Foster, 1993] carried by a SAPS [Foster and Vo, 2002] located equatorward of the duskside midlatitude trough [Rodger *et al.*, 1992]. Thus, we must also discuss the role played by the convection on closed field lines in transporting midlatitude plasma into the cusp inflow

region. Here, we presume that an abnormal expansion of the high-latitude convection system triggered the TOI during this storm event. Then, we estimate how the high-latitude convection expanded equatorward during this storm by using the temporal variation of the PCB as a proxy and try to discuss the possible relationship between the expansion of the high-latitude convection and the appearance of TOI.

[37] In order to estimate the temporal evolution of the PCB, we employ the particle data from all available passes of DMSP and NOAA POES during this storm event. Figures 12a and 12b show the energy spectrograms of electrons and ions observed by DMSP F13 passing through the

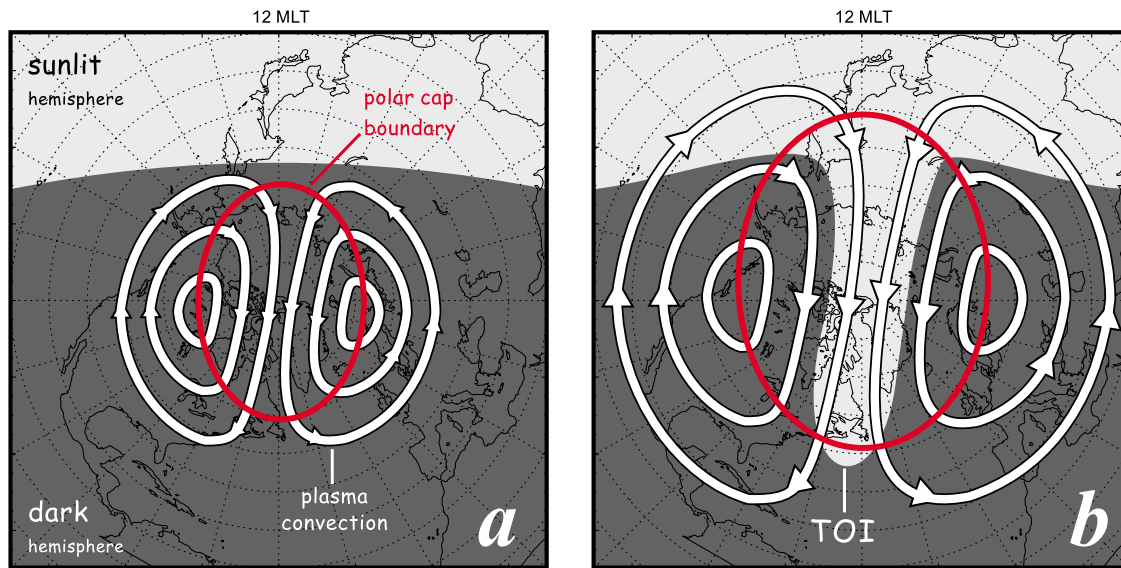


**Figure 11.** Schematic illustrations of the wintertime high-latitude plasma environment during (a) quiet or moderately disturbed and (b) storm conditions. The PCB is indicated by the red circle.

dayside part of the polar cap from dusk to dawn at around 0230 UT on 15 December. In both frames, two clear demarcation lines can be identified between regions of intense particle precipitation and of no precipitation, corresponding to the PCB on the duskside and dawnside, respectively. From this orbit, we locate the MLAT of the PCB at  $65.6^\circ$  on the duskside and  $64.1^\circ$  on the dawnside, as indicated by the dashed lines in the spectrograms. Figures 12c and 12d show integrated fluxes of precipitating electrons and ions in two energy channels (50 eV to 1 keV and 1 keV to 20 keV) obtained from NOAA POES 15 passing through the polar cap from dusk to dawn at around 0415 UT. It is slightly harder to identify the PCB from the NOAA POES data because the fluxes are integrated over broad energy ranges. However, in both frames, signatures of the cutoff of the flux can be identified on both sides of the polar cap, which are manifestations of the PCB in the NOAA POES data. From this orbit, we identified the MLAT of the PCB at  $64.6^\circ$  on the duskside and  $63.8^\circ$  on the dawnside, as indicated by the dashed lines, although it should be noted that the boundaries located from NOAA POES include an uncertainty as large as approximately  $1^\circ$ . We identified 26 PCB signatures between 1800 UT on 14 December and 0600 UT on 15 December from the DMSP and NOAA POES data.

[38] Figure 13d shows the temporal variation of the MLAT of the PCB as estimated from DMSP and NOAA POES during a 12 h interval from 1800 UT on 14 December to 0600 UT on 15 December. The boundaries detected by DMSP (NOAA POES) are indicated by open (solid) circles. Here, note that we only plotted the boundaries located on the dayside (from 06 to 18 MLT) because the PCB on the nightside is generally located a few degrees equatorward of that on the dayside due to its diurnal variation [Feldsten and Starkov, 1967]. The IMF  $B_y$ ,  $B_z$ , and AE index are shown in the three upper panels for the sake of comparison. The duration of the optical plume is again highlighted in grey. Before 2230 UT on 14 December, the boundary stayed above  $75^\circ$ , which is consistent with the northward IMF during this

interval. The boundary abruptly started moving equatorward at around 2230 UT and the MLAT of the boundary was as low as  $60^\circ$  immediately before the onset of the TOI at around 0030–0050 UT on 15 December. That is, the boundary moved equatorward for almost  $15^\circ$  in only 2 h. In general, the size of the PCB is controlled by a balance between the creation and the destruction of open flux in the magnetosphere [Siscoe and Huang, 1985]. The open flux is created by the dayside magnetopause reconnection and it is destroyed by the tail reconnection associated with substorms; thus, both the dayside and nightside reconnection rates determine the temporal variation of the PCB. Milan *et al.* [2003] and Hosokawa *et al.* [2003] demonstrated that increases in the polar cap area occurred when the IMF is oriented southward and low-latitude magnetopause reconnection is ongoing, and decreases in area corresponded to open flux being destroyed at substorm breakup. Hence, the very rapid expansion of the PCB from 2230 UT on 14 December to 0030 UT on 15 December was primarily caused by a bursty creation of open flux due to large negative  $B_z$  after 2200 UT (Figure 13b). During the interval of the TOI, the boundary stayed at around  $64^\circ$ – $66^\circ$ . Figure 13b shows that the IMF  $B_z$  was directed largely negative throughout the interval of TOI; thus, open flux continued to be created. However, the AE index shown in Figure 13c indicates an occurrence of intense substorm activities (AE index  $\approx 2000$  nT); this could reduce the amount of open flux in the polar cap area through the tail reconnection. Hence, the dayside and nightside reconnection rates were almost balanced and the PCB remained at around  $65^\circ$  MLAT throughout the interval of the TOI. After the disappearance of the TOI at around 0500 UT on 15 December, the PCB returned to a higher latitude ( $\approx 70^\circ$ ). Around this time, the IMF  $B_z$  exhibited a northward excursion for approximately 30 min. Hence, the destruction of open flux due to continuing substorm activities caused this poleward motion of the PCB. It should be noted that the extreme expansion of the PCB was completed shortly before the onset of the TOI and the boundary returned to higher latitudes at around the time of the

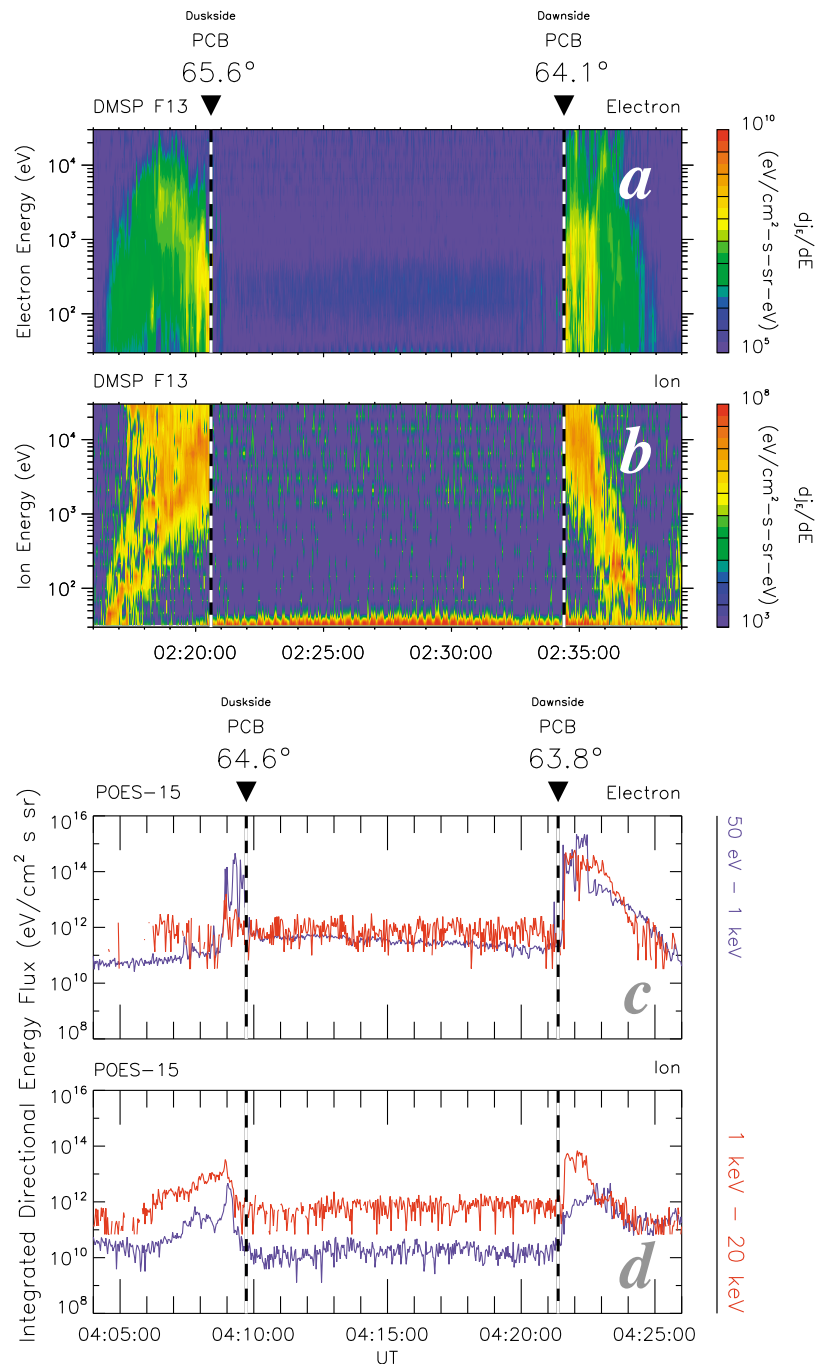


**Figure 12.** (a and b) The energy spectrograms of electrons and ions observed by DMSP F13 passing through the dayside part of the polar cap from dusk to dawn at around 0230 UT on 15 December. (c and d) The integrated fluxes of precipitating electrons and ions in two energy channels (50 eV to 1 keV, blue; 1 keV to 20 keV, red) obtained from NOAA POES 15 passing through the polar cap from dusk to dawn at around 0415 UT.

disappearance of the TOI, suggesting that the expansion/contraction of the high-latitude convection system was one of the factors controlling the appearance/disappearance of the TOI.

[39] Figure 13d suggests that the PCB was located at least as low as  $65^\circ$  MLAT during the TOI event, probably allowing the high-latitude convection system to transport the dense midlatitude plasma into the polar cap as a TOI. Figure 14

again shows the optical data at 0410 UT on 15 December, in which the contours of electric potential derived from SuperDARN are overlaid. The red (blue) line shows the terminator at ground (250 km altitude) level. The green circle indicates the location of the PCB during a quiet period ( $K_p = 2$ ) as estimated from the auroral oval model by *Feldsten and Starkov* [1967]. It is clearly seen that the PCB in a quiet period is located poleward of both the terminators.

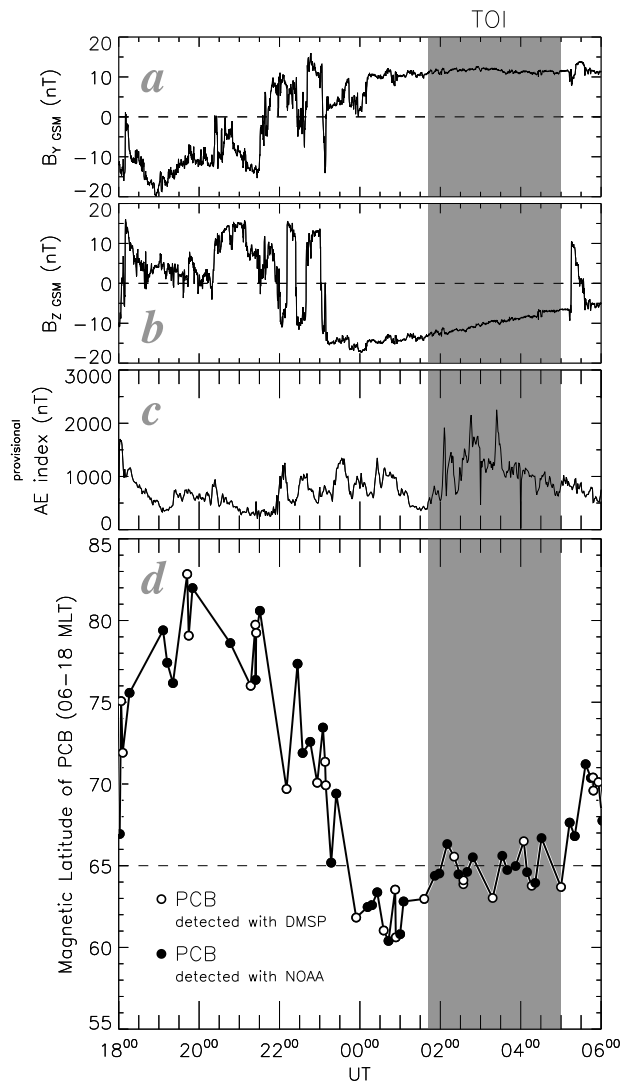


**Figure 13.** (a and b) The IMF  $B_y$  and  $B_z$  obtained from the ACE satellite time shifted to the dayside magnetopause during a 12 h interval from 1800 UT on 14 December to 0600 UT on 15 December. (c) The provisional AE index. (d) The temporal variation of the MLAT of the PCB as estimated from DMSP and NOAA POES. The boundaries detected by DMSP (NOAA POES) are indicated by open (solid) circles.

In such a situation, the polar cap convection cannot interact with the sunlit plasma equatorward of the terminator; thus, the plasma convection cannot contribute to the generation of TOI. The yellow curve indicates the PCB during the TOI as estimated from DMSP and NOAA POES, which is approximately  $10^\circ$  equatorward of its normal position. This extreme expansion of the polar cap area allowed the anti-sunward convection to capture the high-density plasma equatorward of the terminator and transport them into the dark polar cap as a bright optical plume. If we look at the convection streamlines derived from SuperDARN, the lower-latitude boundary of the high-latitude convection system reached  $50^\circ$  MLAT in the duskside sunlit area. Namely, along with the extreme expansion of the PCB, the flow on

closed field lines extended further into the lower latitudes. As will be shown in section 4.2, during the interval of TOI, a SAPS was observed in the lowest-latitude part of the high-latitude convection in the postnoon sector. *Foster et al.* [2007] employed the ionospheric TEC measurements, DMSP ion drift data and IMAGE EUV images to demonstrate that the equatorward edge of the SAPS electric field overlapped the SED plume and that plume material was carried toward the cusp from the SAPS overlap region. Also in the current interval, the SAPS electric field located in the lowest-latitude part of the high-latitude plasma convection system probably captured dense plasma of midlatitude origin and transported it into the cusp inflow region as an SED, as suggested by *Foster* [1993] and *Foster et al.* [2005]. Such an abnormal plasma transport finally contributed to the formation of the TOI during this specific storm event.

[40] The other important point to note is that the evolution of SAPS is not deeply associated with the development of the high-latitude convection system that is directly driven by the solar wind disturbances. A SAPS during a magnetic storm is usually considered as a manifestation of the coupling between the low-conductance subauroral ionosphere and ring current in the inner magnetosphere [*Foster and Burke, 2002*]. When the ring current develops in the inner magnetosphere, a large pressure maximum is formed in the nightside magnetosphere, which causes Region 2 field-aligned currents (R2-FACs) flowing into the ionosphere. Intense poleward-directed electric fields are then set up to drive closure currents flowing poleward across the low-conductivity midlatitude trough in the subauroral region. Within the region of strong plasma drifts, frictional heating enhances ionospheric recombination rates resulting in a reduction of the conductance. Such an ionospheric feedback process can further intensify the polarization electric fields. As long as the pressure gradients associated with the ring current exist, they drive R2-FACs coupling the magnetosphere and ionosphere, and maintain an intense poleward electric field in the subauroral region. Thus, the evolution of SAPS is a consequence of the M-I coupling between the subauroral ionosphere and inner magnetosphere via R2-FAC. This means that the convection pattern observed during the TOI was a result of a convection of the evolution of the main convection cells driven by the solar wind and the SAPS driven by the ring current, suggesting that the evolution of ring current during the storm is important for understanding the abnormal plasma transport and ultimately the formation of the TOI.

[41] As demonstrated above, the extreme expansion of the PCB possibly allowed the SAPS, that was located in the lowest-latitude portion of the high-latitude plasma convection system, to entrain the midlatitude high-density plasma into the dark polar cap ionosphere. However, even if the high-latitude convection system expanded equatorward abnormally, the bright optical TOI could not be generated unless the source plasma at midlatitudes was sufficiently dense. In order to clarify the distribution of the source plasma, we plot the absolute vertical GPS-TEC data during 5 h intervals from 0030 to 0530 UT on 14 and 15 December in Figure 15. The data for 14 December shown in the left-hand side panels were obtained well before the arrival of the shock at around 14 UT on 14 December (Figure 4f); thus, the maps on the left-hand side correspond to the plasma distribution during the quiet period. The TEC values in the daytime midlatitude region

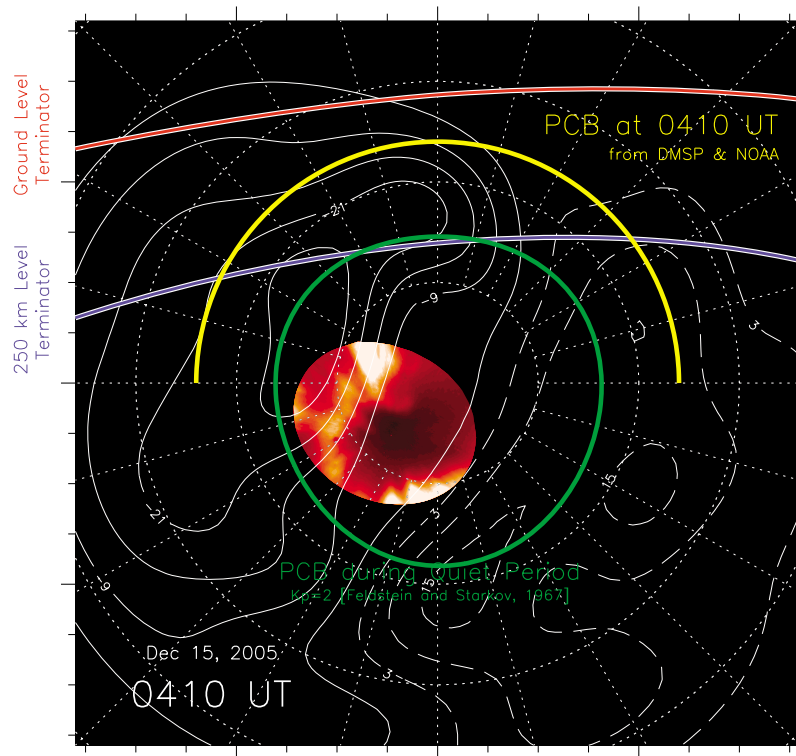


**Figure 14.** A 630.0 nm optical image at 0410 UT on 15 December, in which the contours of electric potential derived from SuperDARN are overlaid. The red (blue) line shows the terminator at ground (250 km altitude) level. The green circle indicates the location of the PCB during a quiet period ( $K_p = 2$ ) as estimated from the auroral oval model by *Feldstein and Starkov* [1967]. The yellow curve indicates the PCB during the TOI as estimated from DMSP and NOAA POES.

(say  $<60^\circ$  MLAT) ranged from 5 to 8 TECU. In contrast, on 15 December, TEC in this region was clearly enhanced as compared to that on the previous day. The TEC values were much greater than 20 TECU, which were at least 3–4 times denser than those in a quiet period. This suggests that a positive ionospheric storm [e.g., *Prölss*, 1995] occurred during the TOI; this made the source plasma sufficiently dense for the generation of the bright optical TOI.

[42] In order to reveal when and how the positive ionospheric storm started, we color coded the GPS-TEC data at 12–13 MLT sector (indicated by the red triangle in Figure 15a) as a function of UT and MLAT in Figure 16c. The horizontal axis is UT from 0000 UT on 14 December to 2400 UT on 15 December and the vertical axis is MLAT. The positive storm shown in Figure 15 (hereafter referred to as “P-S-2”) commenced at around 2320 UT on 14 December, which was immediately after the major southward turning of the IMF  $B_z$  at around 2320 UT, as shown in Figure 16a. An enhancement of the TEC was more prominent in the lower-latitude region ( $20\text{--}50^\circ$  MLAT); however, its effect was observed over a wide range of MLAT from  $20^\circ$  to at least  $70^\circ$ . The TEC values increased up to 40 TECU at  $20\text{--}40^\circ$  MLAT, which was at least 4 times greater than those on the previous day. Ionospheric variations associated with P-S-2 were previously investigated in detail by *Pedatella et al.* [2009], who showed that large enhancements of TEC were observed at latitudes equatorward of  $\approx 70^\circ$  over the Pacific Ocean region during 4 h period from 0000 to 0400 UT on 15 December. They

also indicated that the effect of P-S-2 remained present in the equatorial region beyond 1200 UT. *Lei et al.* [2008b] used the Coupled Magnetosphere Ionosphere Thermosphere (CMIT) model to demonstrate that both equatorward neutral winds and vertical drifts were increased at low to midlatitudes during the initial stage of P-S-2 (0000–0400 UT). Their modeling results suggested that enhanced equatorward neutral winds and upward drifts were responsible for producing the large positive storm effect over the Pacific Ocean region. Figure 9 showed that the signature of the TOI appeared at around 0030–0050 UT on 15 December, which was approximately 1–1.5 h after the onset of P-S-2. This suggests that the TOI plasma originated from the region of enhanced TEC in the midlatitudes associated with P-S-2.

[43] Combination of the DMSP and ASI data demonstrated that the TOI appeared in the polar cap between 0050 to 0500 UT on 15 December. Figure 13d shows that the PCB started moving equatorward at around 2230 UT on 14 December and got across MLAT of  $65^\circ$  at around 2340 UT. P-S-2 commenced at 2320 UT on 14 December. Thus, the TOI started being detected 1–1.5 h after the “expansion of the high-latitude convection system” and “build up of the source plasma in the midlatitudes.” This time difference of 1–1.5 h could be attributed to the time required for transporting midlatitude plasma to the polar cap region. If we assume that the source plasma was distributed at  $60^\circ$  MLAT and a TOI was first observed at  $80^\circ$  MLAT on the dayside, the distance between these two points along the convection

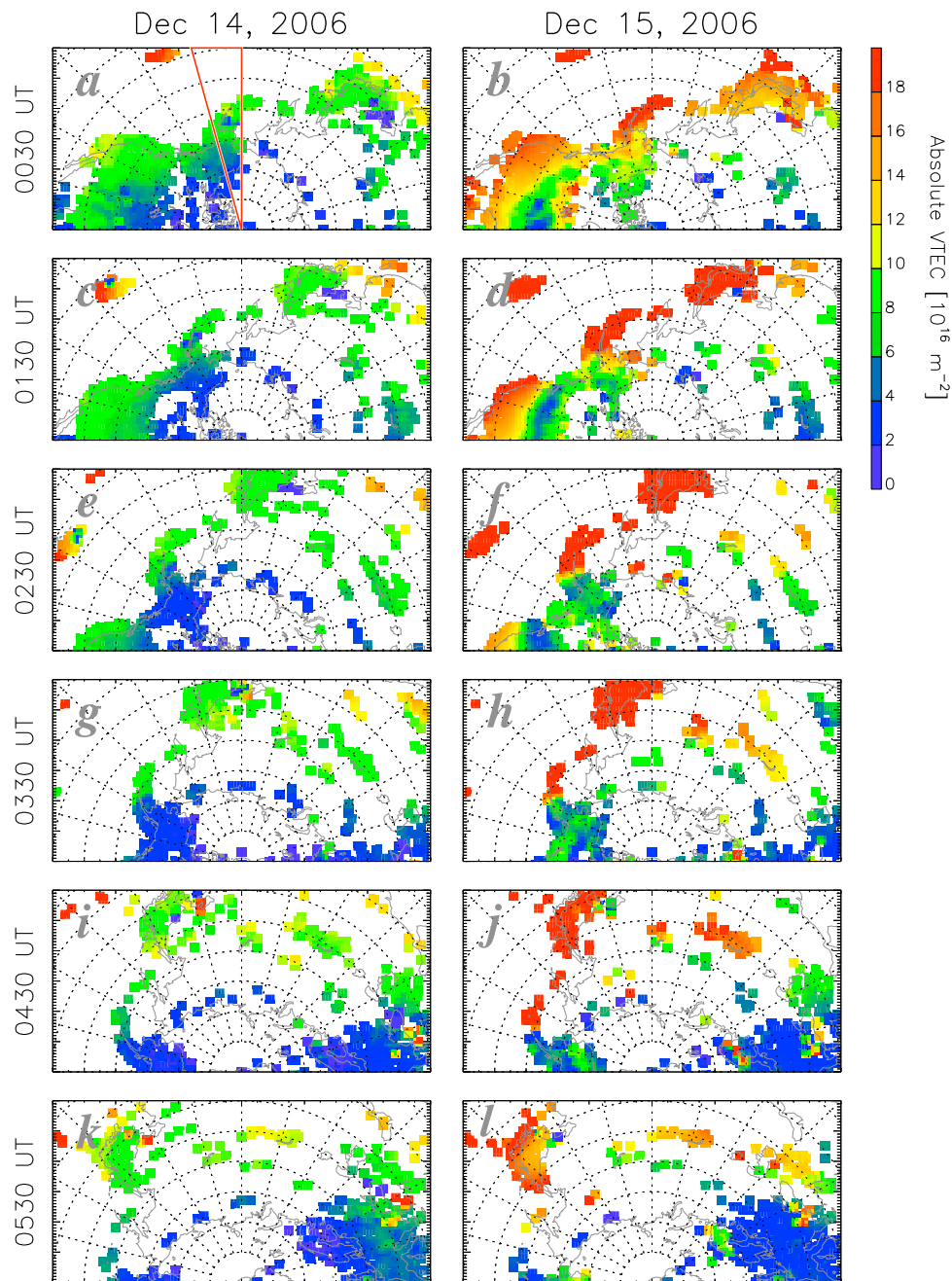


**Figure 15.** The absolute vertical GPS-TEC data during 5 h intervals from 0030 to 0530 UT on (left) 14 December and (right) 15 December.

streamline as shown in Figure 14 could be around 3000–4000 km. The convection speed within the TOI as inferred from the DMSF ion drift data shown in Figure 7e was approximately  $800 \text{ m s}^{-1}$ . Thus, it could take 1–1.5 h to transport the source plasma from midlatitude to the polar cap region, which can account for the time difference between the appearance of TOI and the two factors leading to the formation of TOI. In this example, the two necessary conditions for generating TOI, “expansion of the high-latitude convection system” and “build up of the source plasma in the midlatitude,” were satisfied almost simultaneously because both of them were triggered by the major southward turning of the IMF at 2230 UT on 14 December. Then, the TOI promptly

started being generated and extended into the polar cap. This directly indicates that the prolonged large-amplitude southward IMF  $B_z$  in the later part of the magnetic cloud was ultimately responsible for producing the TOI during this magnetic storm.

[44] As suggested by *Pedatella et al.* [2009], Figure 16c shows that the effect of P-S-2 continued to be seen at least until 1200 UT on 15 December in the lower-latitude region ( $<40^\circ$  MLAT). However, if we look at the data at  $20\text{--}40^\circ$  MLAT in the first few hours of P-S-2, the significant increase in TEC greater than 40 TECU almost ceased at around 0340 UT. This implies that the highlight of P-S-2 was approximately 4 h from 2320 UT on 14 December to

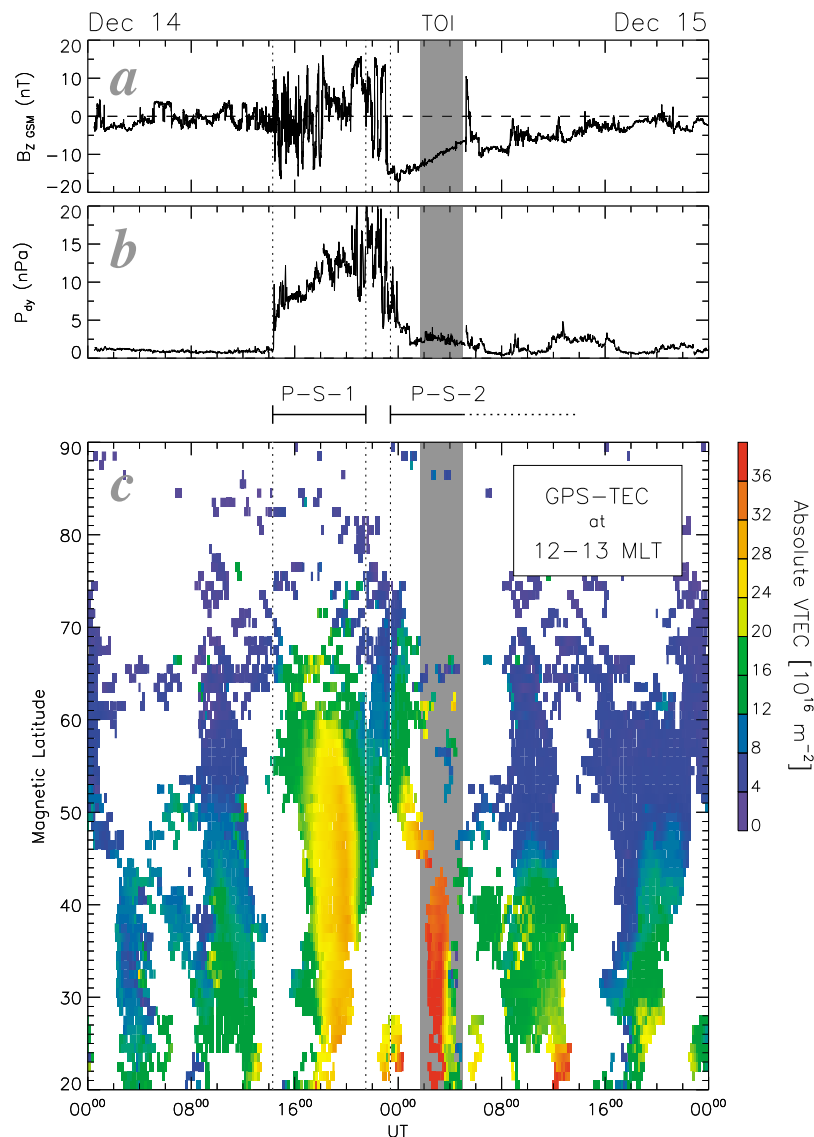


**Figure 16.** (a and b) The IMF  $B_z$  and solar wind dynamic pressure obtained from the ACE satellite time shifted to the dayside magnetopause during a 48 h interval from 0000 UT on 14 December to 2400 UT on 15 December. (c) GPS-TEC data at 12–13 MLT sector as a function of UT and MLAT.

0340 UT on 15 December. It should be noted that the disappearance of the TOI occurred just 1–1.5 h after the termination of the significant increase in TEC in the low-latitude to midlatitude region at around 0340 UT on 15 December. Again, the time delay of 1–1.5 h between the disappearance of TOI and termination of the significant TEC enhancement in the lower-latitude region could be attributed to the time required for transporting midlatitude plasma to the polar cap region. This suggests that the TOI stopped being observed because the source plasma in the dayside lower latitude was no longer sufficiently dense after 0340 UT. Thus, the disappearance of the TOI was more likely to be caused by the temporal variation of the source plasma in the daytime midlatitude regions.

[45] Another point to mention is that another positive storm occurred well before the onset of the TOI, indicated as “P-S-1” in Figure 16c. P-S-1 started at around 1400 UT

soon after the arrival of the shock to the dayside magnetopause (Figure 16b). The signature of P-S-1 was observed as an increase in TEC up to 30 TECU in a wide range of MLAT from 20° to 70°. The details of P-S-1 have already been reported by *Lei et al.* [2008a], who claimed that changes in the electric field associated with fluctuations in IMF  $B_z$  played a dominant role in generating the large enhancement of TEC during P-S-1 although neutral winds and composition changes also contributed. Thus, the processes responsible for producing P-S-1 and P-S-2 were somewhat different although they exhibited some similarities in the structure of the positive storm effects. Figure 16c shows that the effect of P-S-1 continued to be observed for approximately 8 h from 1400 until 2140 UT. However, the DMSP data shown in Figures 9a and 9h demonstrate that no signature of a TOI was detected within the 4.5 h from 2000 UT on 14 December to 0030 UT on 15 December; thus, a TOI was not generated

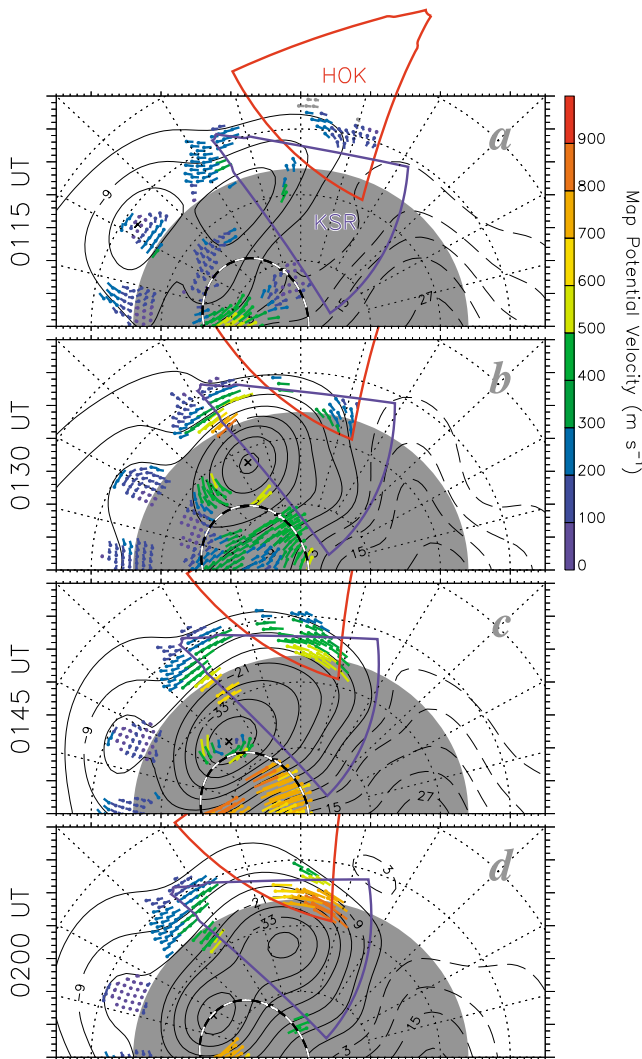


**Figure 17.** The convection maps derived from the Northern Hemisphere SuperDARN data in every 15 min from 0115 to 0200 UT on 15 December on which the FOVs of the SuperDARN Hokkaido and King Salmon radars are superimposed.

during P-S-1. This suggests that a TOI cannot always form even if the density of the source plasma is increased by positive storm effects. As shown in Figure 13d, the PCB was located above  $75^\circ$  MLAT during the interval of P-S-1, implying that the plasma convection system was probably confined to the dark hemisphere in higher latitudes. This did not allow the source plasma in the midlatitude to be transported to the polar cap area as a TOI, again suggesting that both “expansion of the high-latitude convection” and “occurrence of positive storm” are necessary conditions for the formation of large-scale transpolar TOI.

#### 4.2. What Caused the Dynamic Motion of the TOI?

[46] As shown in Figure 8, after the appearance at around 0140 UT, the TOI moved back and forth in the dawn to dusk direction very dynamically. In particular, the TOI suddenly started moving downward at around 0250 UT and shifted its location by approximately 1000 km in some 15 min. The

DMSP ion density data plotted in Figure 9 also demonstrate that the TOI actually changed its position dawnward at around this time period. Here, we discuss what physical process caused this motion in detail. One may suspect that the downward excursion of the TOI was simply due to a change in the convection pattern on open field lines (i.e., in the polar cap region) associated with reorientation of the IMF  $B_y$ . If we had a large-scale change in the IMF  $B_y$  from negative to positive, the dusk cell could expand dawnward [e.g., Weimer, 2005; Ruohoniemi and Greenwald, 2005], and then, the TOI in the central polar cap would move in the same direction. However, the IMF data plotted in Figures 4b and 4c show no outstanding drastic change in IMF  $B_y$  and  $B_z$  during the TOI, implying that the plasma convection on open field lines did not vary very much. That is, the streamline of the polar cap convection remained almost stable throughout the TOI event. Hence, the change in IMF  $B_y$  is unlikely to contribute to the rapid downward excursion of the TOI starting at around 0250 UT.

[47] Now, we focus on the convection on closed field lines. Figure 17 shows the convection maps derived from the Northern Hemisphere SuperDARN data every 15 min from 0115 to 0200 UT on 15 December. The grey region indicates an average polar cap extent during the TOI as estimated from DMSP and NOAA POES (MLAT of the PCB  $\approx 66^\circ$ ). After 0130 UT, a strong westward flow appeared on closed field lines (i.e., outside the PCB) around 14 MLT. Subsequently, this flow burst on closed field lines progressed westward and finally penetrated deep into the nighttime subauroral region at 0200 UT. The maximum speed of this westward flow was as high as  $1 \text{ km s}^{-1}$ . It is important to note that this flow burst and the FOV of the ASI at Resolute Bay (indicated by the dashed circle in Figure 17) were sitting on the same contours of the convection streamline connecting the duskside subauroral region to the polar cap region through the cusp inflow region. This indicates that the westward flow burst on closed field lines was probably responsible for delivering the source plasma of TOI from the duskside midlatitude to the noontime cusp inflow region, which is consistent with the picture proposed by Foster *et al.* [2005], who showed that the source of transpolar TOIs was SEDs carried by SAPS from the duskside midlatitude region. We speculate that the westward flow burst on a closed field line was directly associated with SAPS penetrating from the duskside. Then, we suggest that the westward progression of the SAPS flow after 0130 UT changed the location of the source of TOI (i.e., SED) dawnward and finally caused the downward excursion of the TOI in the central polar cap area. The MLAT of the westward flow was approximately  $63^\circ$ – $65^\circ$ , which was well equatorward of most of the SuperDARN radars in the auroral zone. However, fortunately, the second midlatitude SuperDARN radar in Hokkaido started operating just 1 month before this storm event, which allowed us to monitor the flow on closed field lines. In addition, another Japanese SuperDARN radar in King Salmon, Alaska, captured some backscatter echoes associated with this westward flow. The FOVs of these two radars are superimposed on the convection maps in Figure 17. In the next part, we describe the details of the Doppler velocity observations made by these radars.

[48] Figure 18a shows the backscatter power from beam 0 of the Hokkaido radar in the format of Range-Time-Intensity

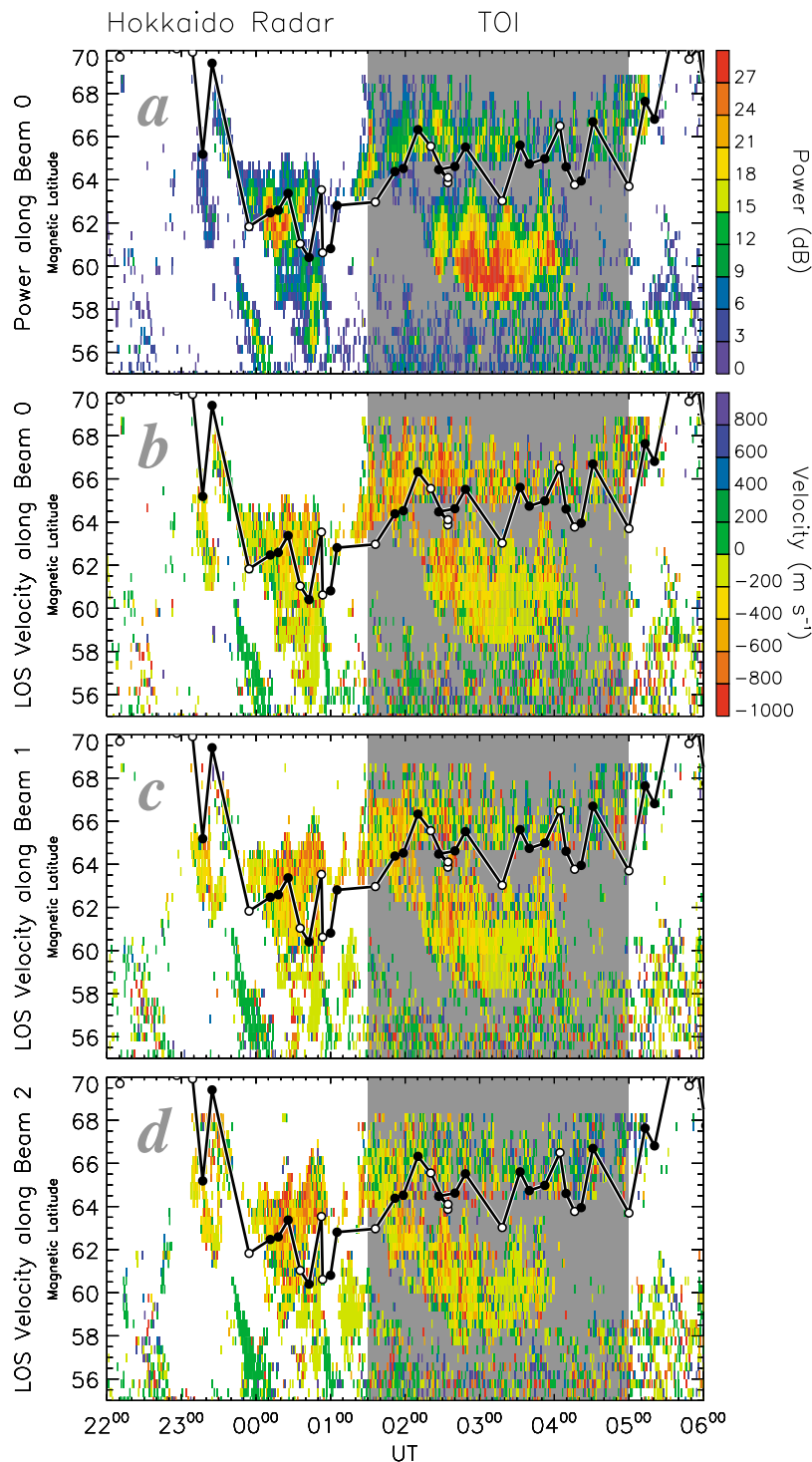


**Figure 18.** (a) The backscatter power from beam 0 of the SuperDARN Hokkaido radar in the format of Range-Time-Intensity (RTI) plot. The black line superimposed on the RTI plot gives the location of the PCB as estimated from DMSP and NOAA POES. (b–d) The line-of-sight Doppler velocity data from beam 0, 1, and 2 of the Hokkaido radar in the RTI format.

(RTI) plot. Beam 0 (western-most beam) of Hokkaido is directed roughly toward the magnetic north; thus, it is suitable for observing the poleward component of the flow in this region. The black line superimposed on the RTI plot gives the location of the PCB as estimated from DMSP and NOAA

POES. The radar observed lots of backscatter echoes during the TOI both poleward and equatorward of the PCB. Figures 18b, 18c, and 18d show the line-of-sight Doppler velocities obtained from beams 0, 1, and 2, respectively, of the Hokkaido radar. The broad echo region equatorward of

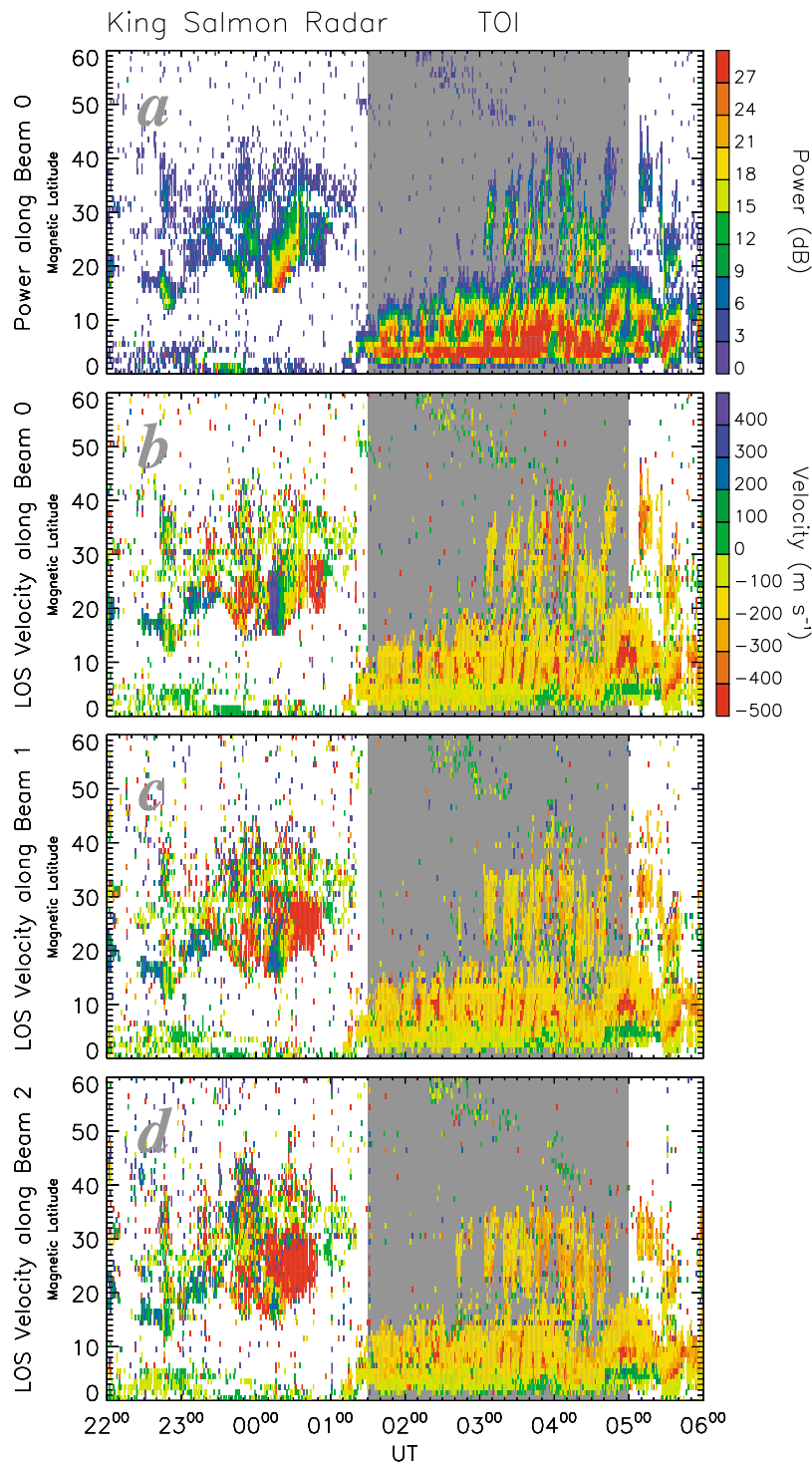


**Figure 19.** (a) The backscatter power from beam 0 of the SuperDARN King Salmon radar in the format of Range-Time-Intensity (RTI) plot. (b–d) The line-of-sight Doppler velocity data from beam 0, 1, and 2 of the King Salmon radar in the RTI format.

the PCB corresponds to the westward flow on closed field lines shown in Figure 17. The Doppler velocities obtained from this region were mostly away from the radar, implying that the westward flow on closed field lines had some poleward component. In addition, the flow equatorward of the PCB was distributed to an extremely lower latitude as low as  $58^\circ$  MLAT.

These observational facts indicate that the flow on closed field lines could contribute to the plasma transport from the mid-latitude to the cusp inflow region. Figure 19 shows the data from King Salmon in the same format as that in Figure 18; however, the vertical axis is not MLAT but the radar range gate. Beams 0, 1, and 2 (western-most three beams) of King

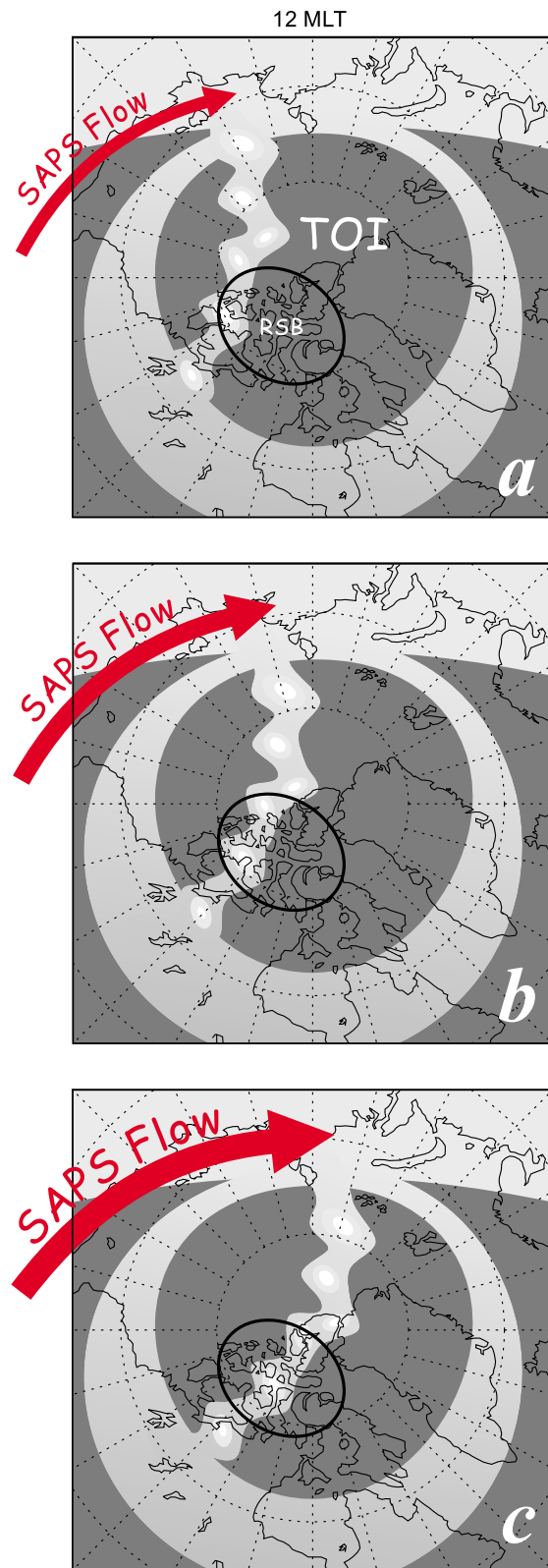


**Figure 20.** (a–c) Schematic illustrations showing how the westward progression of the SAPS-associated flow contributed to the dawnward excursion of the TOI in the central polar cap.

Salmon are directed westward, as shown in Figure 17; thus, they are more suitable for observing westward directed flow. The radar started observing echoes in the range gates 5–20 at around 0130 UT, which well corresponded to the appearance of the westward flow in the convection maps. The Doppler velocities were away from the radar, which is equivalent to westward directed flow in this local time sector. The data from King Salmon again suggest that some rapid westward flows appeared at around 0130 UT in the postnoon sector and the flow probably transported the midlatitude dense plasma into the cusp inflow region as a source of the transpolar TOI over Resolute Bay. Interestingly, the radar observed lots of pulsed enhancements of the flow speed during the TOI, which will be discussed in relation to the mesoscale structure of the TOI in section 4.3.

[49] As mentioned above, the SuperDARN data show that westward progression of plasma flow on closed field lines (possibly SAPS) occurred during 30 min from 0130 UT to 0200 UT, which is approximately 1 h before the dawnward excursion of the TOI in the central polar cap. We also suggest that the westward flow was responsible for transporting the midlatitude plasma to the cusp inflow region. If the flow on closed field lines penetrates further into the dayside (i.e., progresses westward), the possible entry point of the SED plasma into the polar cap should be shifted dawnward accordingly. Such a dawnward motion of the entry point of the SED plasma could lead to the dawnward excursion of the TOI in the central polar cap area. Figure 20 schematically illustrates this scenario. Before the westward progression of the SAPS-associated flow occurred, the entry point of the SED into the polar cap was located on the postnoon area (Figure 20a). In this situation, the transpolar TOI was located on the duskside part of the polar cap and its optical signature was observed near the duskside edge of the FOV of the ASI at Resolute Bay. After the SAPS-associated flow started penetrating into the dayside, the SED plasma also changed its entry point dawnward and the TOI shifted its sitting location accordingly (Figure 20b). Finally, the SAPS flow penetrated further into the dayside and the optical signature of the TOI was observed in the middle of the FOV of the ASI at Resolute Bay. This scenario can explain the time delay between the westward progression of the SAPS-associated flow on the dayside and the dawnward motion of the TOI in the central polar cap. Even if the entry point of the SED plasma into the polar cap changed by the westward progression of the SAPS flow, it took some time to transport them deep into the central polar cap area over Resolute Bay. The distance between the cusp inflow region at around  $66^\circ$  MLAT and the FOV of the ASI at Resolute Bay was approximately 3000 km. If we assume the speed of the polar cap convection to be  $800 \text{ m s}^{-1}$  (an average of the Doppler velocities observed by the Hokkaido radar poleward of the PCB), it would take approximately 1 h to transport the SED plasma entering the cusp inflow region into the FOV of the ASI at Resolute Bay. Thus, the dawnward excursion of the TOI occurred approximately 1 h after the progression of the SAPS-associated flow started on the dayside. The scenario shown in Figure 20 suggests that global circulation of plasma including flows on closed field lines controls the temporal evolution of TOI during this specific magnetic storm.

[50] We suspect that the westward progression of the flow on closed field lines was related to a sunward extension of

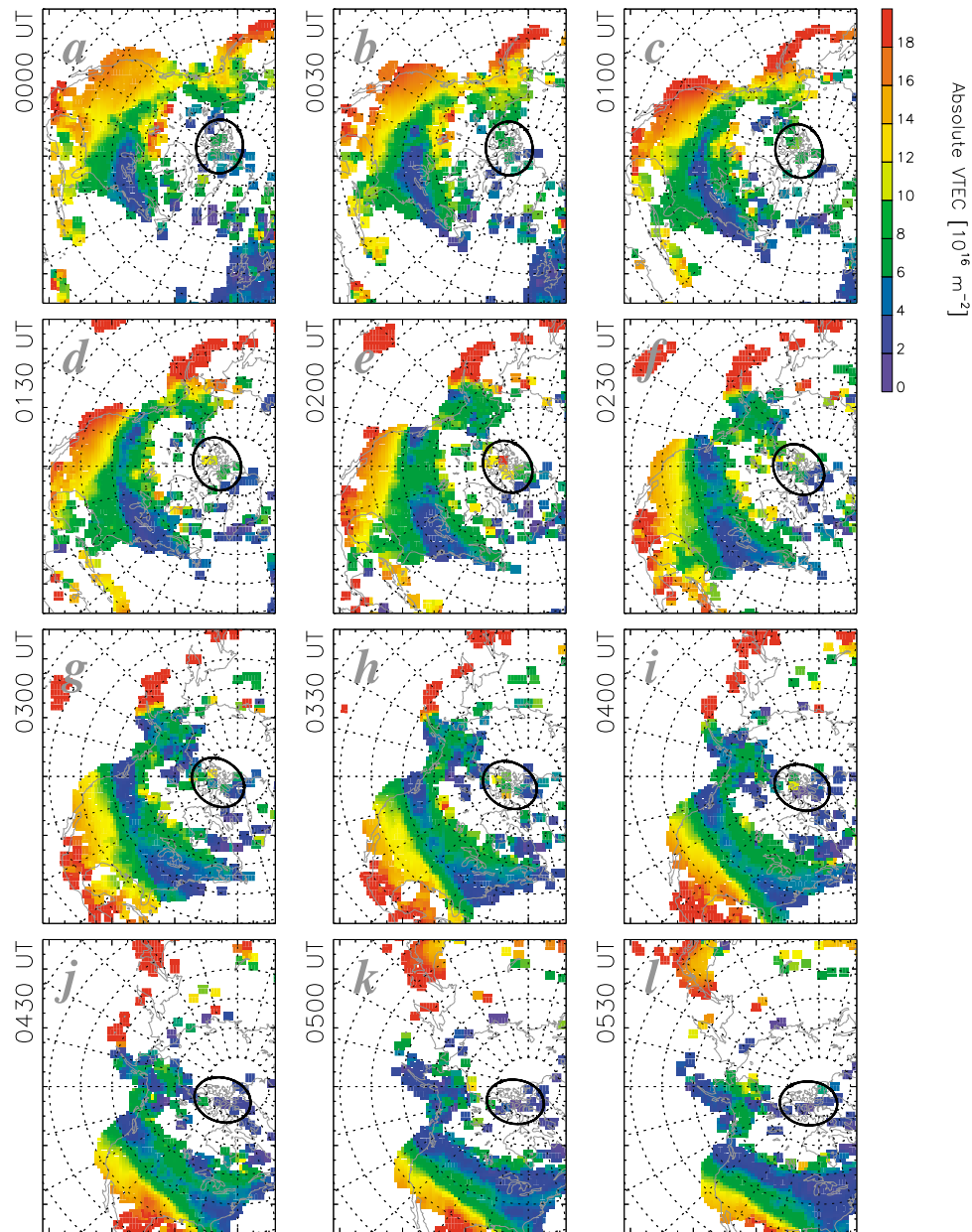


**Figure 21.** A sequence of the GPS-TEC maps every 30 min during 5.5 h from 0000 UT to 0530 UT on 15 December. The FOV of the ASI at Resolute Bay is indicated by the black circle.

the SAPS from the duskside. In other words, the westward flow corresponds to the sunward leading edge of the SAPS. Such a type of sunward extension of a SAPS have never been reported in the past literature because SAPSs have usually been observed by LEO satellites such as DMSP. However, *Hosokawa et al.* [2001, 2002] used the SuperDARN radar data to show that the sunward edge of the midlatitude trough on the duskside tends to extend to an earlier local time sector during disturbed conditions. Because SAPSs generally overlap with the midlatitude trough [*Foster and Vo, 2002; Basu et al., 2008*], it could also extend into the dayside together with the trough during disturbed conditions. Here, we try to show the temporal evolution of SAPS by using the signature of the trough in the GPS-TEC maps. Figure 21 shows a sequence of

the GPS-TEC maps every 30 min during 5.5 h from 0000 UT to 0530 UT on 15 December. A clear signature of the midlatitude trough can be seen as a region of decreased TEC on the duskside. As the midlatitude trough is closely associated with a SAPS, the spatial extent of the trough is a good proxy for identifying the structure of a SAPS. At 0000 UT, the sunward edge of the trough was in somewhere around 16 MLT. Subsequently, the trough started extending toward the dayside and finally penetrated deep into the dayside sunlit area at 0200 UT. This penetration of the trough was possibly associated with the sunward extension of SAPS.

[51] In order to examine the temporal evolution of the trough and SAPS in more detail, the GPS-TEC data are presented in the format of MLT versus MLAT in Figures 22a–22j, which

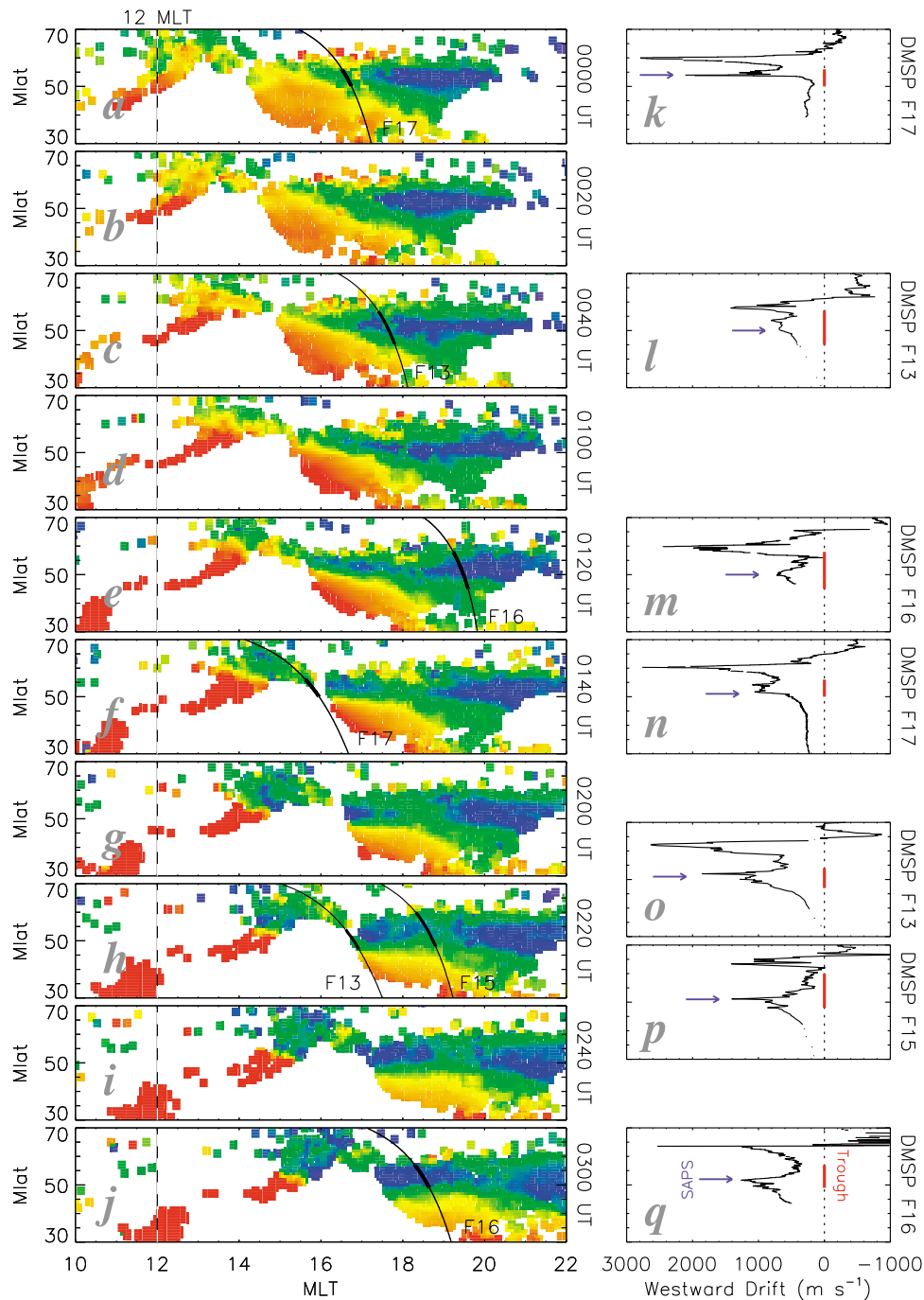


**Figure 22.** (a–j) The GPS-TEC data in every 20 min from 0000 UT to 0300 UT on 15 December plotted in the format of MLT versus MLAT. In some of the frames in Figure 22 (left), orbits of DMSAP passing across the duskside trough are superimposed. The thick black part along the orbit indicates the latitudinal width of the trough estimated from the TEC data. (k–q) The cross-track ion drift data from the DMSAP orbits shown in Figure 22 (left). The thick red line shows the width of the trough as estimated from the TEC data. Rapid flows associated with SAPS are indicated by the blue arrows.

is useful for tracking how the trough and SAPS extended into the dayside during the TOI. Although it is not so easy to locate the longitudinal extent of the trough, here we employ the level of 6 TECU (boundary between bluish and greenish colors) as a proxy for its sunward leading edge. Before 0040 UT (Figures 22a, 22b, and 22c), the leading edge of

the trough was located somewhere around 17 MLT. At around 0100 UT or 0120 UT (Figures 22d and 22e), the trough started extending into the earlier local time sector. This extension of the trough appeared to finish at around 0200 UT (Figure 22g). At this time, region of decreased TEC (<6 TECU; bluish pixels) can be seen between 14 and 16 MLT, suggesting that

the leading edge of the trough reached at least around 14 MLT. That is, the sunward edge of the trough shifted for approximately 2–3 MLT in some 40 min. In some of the frames in Figure 22 (left), orbits of DMSP spacecraft passing across the duskside trough are superimposed. The thick black part along the orbit indicates the latitudinal width of the trough estimated from the TEC data. In Figures 22k–22q, the cross-track ion drift data from the DMSP orbits shown in Figure 22 (left) are presented. The thick red line shows the width of the trough as estimated from the TEC data. The ion drift data show that an intense westward flow greater than  $1 \text{ km s}^{-1}$  existed well equatorward of the sunward flow in the main auroral oval. These rapid flows within the trough, as indicated by the blue arrows, correspond to the SAPS. It is well demonstrated that the location of the trough corresponds to that of the SAPS. This supports the one-to-one correspondence between the mid-latitude trough and SAPS during this interval; thus, the sunward extension of the trough demonstrated from the GPS-TEC data was caused by the penetration of the SAPS electric field deep into the dayside ionosphere. This penetration of the SAPS was responsible for the westward progression of the flow on closed field lines observed by the SuperDARN and finally contributed to the rapid downward excursion of the TOI plume in the central polar cap. As mentioned in the previous part, the formation of SAPS is closely associated with the development of ring current. Thus, we suppose that the presented sunward progression of the SAPS was caused by the development of the asymmetric ring current. As the ring current progressed toward the earlier local time sector in the inner magnetosphere, a band of R2-FACs flowing into the subauroral ionosphere could penetrate into the dayside. To close the R2-FACs via poleward flowing Pedersen current, the SAPS also progressed toward the earlier local time. Thus, the longitudinal evolution of the asymmetric ring current in the inner magnetosphere probably played an important role in the dawnward excursion of the TOI in the central polar cap, again suggesting that a global system perspective is needed to understand the observed dynamic features.

#### 4.3. What Determined the Spatial Structure of the TOI?

[52] The 2-D imaging capability of the ASI at Resolute Bay revealed the following spatial characteristics of the TOI during the magnetic storm on 15 December 2006: (1) the TOI was an almost continuous stream of high-density plasma, (2) the TOI contained some mesoscale structures, whose spatial extent ranged from 250–600 km, within itself. Here, we address two questions concerning the characteristics introduced above: “Why did the TOI remain as a continuous stream without being broken into patches?” and “What imposed the mesoscale structures on the main body of the TOI?”.

[53] First, we discuss why the TOI remained as a continuous stream without being broken into patches. During moderately disturbed conditions (i.e., moderate southward IMF conditions during nonstorm time), polar cap patches, rather than TOI, are frequently observed in the polar cap. Although TOI is known as a major source of patches, an occurrence of transpolar large-scale TOI appears to be very rare. In reality, the TOI reported in this paper is the only example that was detected at Resolute Bay since the ASI started its operation in January 2005. Such a low occurrence

of TOIs is probably because they are typically broken into discrete patches before being transported deep into the central polar cap. There are several proposed processes through which daytime dense plasmas are detached from continuous TOI as discrete patches, such as the IMF controlled reorientation of the cusp inflow region [Moen *et al.*, 2008], bursty plasma transport from the subauroral latitudes [Moen *et al.*, 2006], in situ plasma reduction under an intense electric field [Ogawa *et al.*, 2001], and expansion of polar cap convection driven by pulsed reconnection [Carlson *et al.*, 2004]. All the suggested mechanisms commonly employ temporal variations of plasma convection near the cusp to break a TOI into smaller-scale patches. Such types of temporal variations of the cusp plasma flow are associated with the temporal variation of the IMF  $B_y$  and  $B_z$ . Therefore, if there exist some fluctuations in the IMF orientation the TOI should be broken into patches before penetrating deep into the central polar cap and cannot survive as a continuous stream of high-density plasma. The IMF  $B_y$  and  $B_z$  during the TOI (Figures 4b and 4c) show that the direction of the IMF was stable throughout the TOI event although its magnitude was large. This is essentially because this interval corresponds to the phase of slowly rotating IMF in the trailing part of the magnetic cloud.  $\Delta|B|$  shown in Figure 4d also indicates that the magnetic field fluctuation level was quite low during the TOI event. During such an interval of steady IMF orientation, the SED entering into the cusp inflow region was not broken into patches by the temporal variations of the plasma flow on an open field line and it could penetrate deep into the polar cap as it was. That is, the very stable IMF orientation in the latter part of the CME-driven magnetic storm is a key factor allowing the TOI to survive without being broken into discrete patches.

[54] Next, we suggest some processes through which mesoscale patterns were imposed on the main body of the TOI plume. As shown in Figures 4b and 4c, the orientation of the IMF was almost stable throughout the TOI event. This suggests an absence of large-scale changes in the plasma convection pattern near the cusp inflow region. However, if we look at the RTI plots from the Hokkaido and King Salmon SuperDARN radars (Figures 18 and 19), some smaller-scale temporal variations can be identified in the Doppler velocity data both poleward and equatorward of the PCB during the TOI. In order to investigate these variations in greater detail, we plot the Doppler velocity data during the TOI (0030 UT to 0530 UT on 15 December) as a time series in Figure 23. The velocities plotted in Figure 23a are sampled from gate 68 along beam 0 of Hokkaido, that was located poleward of the PCB. Even during the steady IMF conditions, the Doppler velocity data contained some small-scale fluctuations, which could be an ionospheric signature of pulsed reconnection or a so-called flux transfer event [Russell and Elphic, 1978] on the dayside equatorial magnetopause [e.g., Milan *et al.*, 2000; Wild *et al.*, 2003]. These variations do not always result in the large-scale deformation of the convection pattern near the cusp; thus it could not modify the large-scale structure of the TOI plume. However, small-scale fluctuation of the plasma flow associated with pulsed reconnection could impose some mesoscale structures on the main body of the TOI.

[55] Figures 23b and 23c show the Doppler velocity data from gate 50 along beam 0 of Hokkaido and gate 8 along

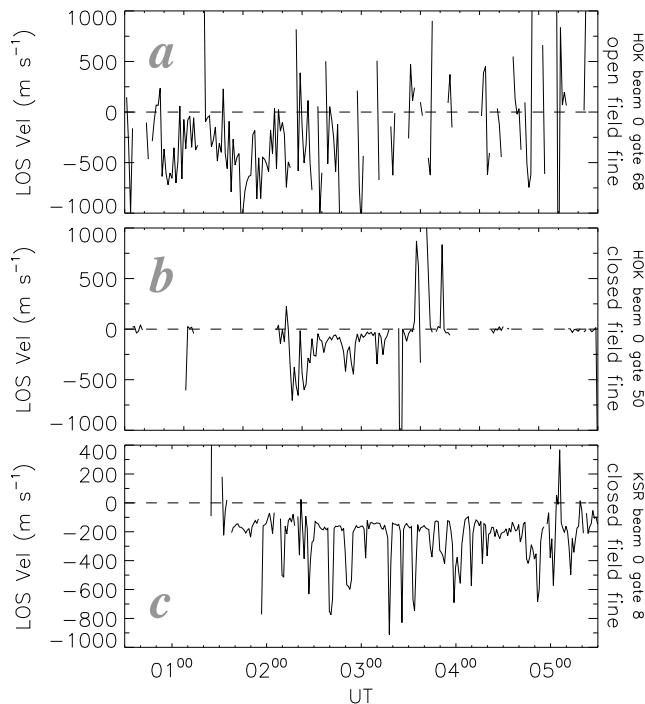


**Figure 23.** (a) The Doppler velocity data during the TOI (0030 UT to 0530 UT on 15 December) as a time series. The velocities plotted here are sampled from gate 68 along beam 0 of Hokkaido, which was located poleward of the PCB. (b and c) The Doppler velocity data from gate 50 along beam 0 of Hokkaido and gate 8 along beam 0 of King Salmon, both of which were located equatorward of the PCB.

beam 0 of King Salmon, respectively, both of which were located equatorward of the PCB (i.e., on a closed field line). Even in the region of closed field lines, the obtained Doppler velocities were found to fluctuate throughout the TOI event. As is more clearly seen in the King Salmon data (Figure 23c), the period of the velocity fluctuation was approximately 5–10 min. In addition, the King Salmon radar data in the RTI plot (Figure 19) demonstrate that these fluctuations clearly propagated away from the radar (i.e., westward). Foster *et al.* [2004] reported wave-like oscillations with 200–300 s periodicity in the electric field magnitude propagating across the SAPS channel. A similar quasiperiodic variation of  $\approx 10$  min periodicity was also observed by Mishin *et al.* [2002]. Streltsov and Foster [2004] and Mishin *et al.* [2003] suggested that an ionospheric feedback instability triggered by the interaction of the large amplitude SAPS field with the low Pedersen conductance in the subauroral region leads to the formation of small-scale intensification of the electric field in the SAPS channel. We could not exactly determine what processes generated the Doppler velocity fluctuation in the SuperDARN data on closed field lines. However, temporal variation of the subauroral plasma flow from dusk to noon sector could modulate the spatial structure of SED and finally could contribute to the formation of the mesoscale structures of the TOI.

[56] Another possible source of the mesoscale structures within the TOI is an ionization caused by particle precipitation. In general, dayside cusp precipitation is too weak to

explain the ionization causing the substructures of TOI. However, during an intense storm, precipitation near the PCB, particularly on the dayside, could enhance the electron density within a TOI before it enters into the polar cap, and temporal variations of precipitation might then be able to modulate significantly the density of convecting plasma, therewith causing some mesoscale structuring within the TOI. Such an effect of particle precipitation on the generation of polar cap patches was previously suggested MacDougall and Jayachandran [2007] who explained the formation of patches and most of their properties by low-energy precipitation into the return flow region. In actual, the DMSP particle data shown in Figure 7d indicate that electron precipitation was quite intense at the edges of the polar cap. We evaluate how much such precipitating electrons could enhance the electron density at the *F* region altitudes by using the energy-range method introduced by Rees [1963]. As a result of the estimation using the DMSP F13 data shown in Figure 7d, the production rate at 250 km altitude is an order of  $10^{10} \text{ m}^{-3} \text{ s}^{-1}$ . The spatial extent of the region of the intense electron precipitation seen just equatorward of the polar cap boundary (around 04:03:30 UT) was about 40 km along the DMSP orbit. If we assume that the convection speed within the TOI was around  $1 \text{ km s}^{-1}$ , it took 40 s for the TOI plasma to pass through the region of intense precipitation. Thus, the electron density within the TOI would be enhanced by  $4 \times 10^{11} \text{ m}^{-3}$  during the passage. Such an enhancement of the *F* region density could contribute to the formation of the mesoscale structures within the TOI.

## 5. Summary and Conclusions

[57] In this paper, we investigate the temporal evolution and spatial structure of a polar cap tongue of ionization (TOI) detected by an all-sky imager (ASI) in the northern part of Canada at Resolute Bay ( $74.73^\circ\text{N}$ ,  $265.07^\circ\text{E}$ ; AACGM latitude  $82.9^\circ$ ) during an intense CME-driven magnetic storm (minimum  $D_{st} = -146 \text{ nT}$ ) on 14–16 December 2006. Figure 24 summarizes the observations presented in this paper, in which the IMF  $B_z$ , solar wind dynamic pressure, AE index, keogram of the 630.0 nm emission along dusk to dawn cross section, keogram of the GPS-TEC data at 12–13 MLT, the magnetic latitude of the polar cap boundary, the line-of-sight Doppler velocities from the SuperDARN Hokkaido and King Salmon radars are displayed for 24 h interval from 1200 UT on 14 December to 1200 UT on 15 December 2006. Here, important findings regarding the dynamic temporal evolution and spatial structure of the TOI are summarized by showing the data in Figure 24.

[58] 1. The optical signature of a TOI was detected in the central polar cap for approximately 3.5 h from 0140 to 0500 UT on 15 December 2006. It was observed as a narrow and bright 630.0 nm airglow plume elongated in the noon-midnight direction almost continuously (Figure 24d).

[59] 2. The ion density measurements from the DMSP satellites passing through the dayside polar cap show that the TOI appeared in the polar cap slightly earlier at around 0050 UT and continued for approximately 4 h until around 0500 UT.

[60] 3. The interval of the TOI corresponded to a period of prolonged large-amplitude southward IMF (Figure 24a) and low solar wind pressure (Figure 24b) in the trailing part of

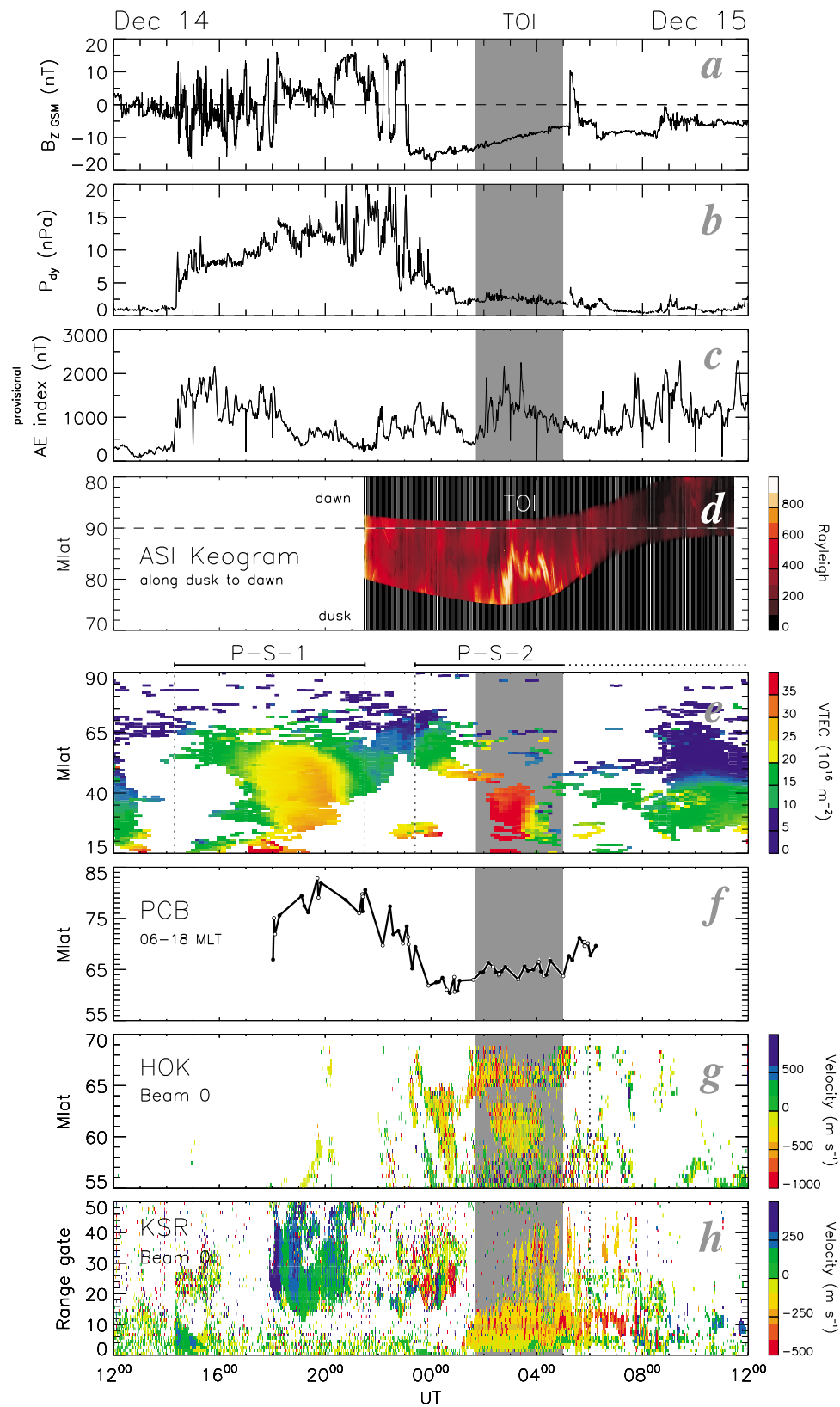


**Figure 24.** Summary of the observational data presented in this paper, in which (a) the IMF  $B_z$ , (b) solar wind dynamic pressure, (c) AE index, (d) the keogram of the 630.0 nm emission along dusk to dawn cross section, (e) the keogram of the GPS-TEC data at 12–13 MLT, (f) the magnetic latitude of the PCB, and (g and h) Doppler velocities of the SuperDARN Hokkaido and King Salmon radars are displayed for a 24 h interval from 1200 UT on 14 December to 1200 UT on 15 December.

the magnetic cloud associated with a CME. There were no turbulent fluctuations in the IMF  $B_y$  and  $B_z$  throughout this period.

[61] 4. The absolute optical intensity of the TOI plume was at least 500 R, which is much brighter than that of non-stormtime polar cap patches. This suggests that the source of the plume could be the solar-produced high-density  $F$  region plasma distributed in the daytime midlatitudes.

[62] 5. The polar cap boundary (PCB) started expanding equatorward across the  $F$  region terminator (Figure 24f) after the IMF directed southward at around 2230 UT on 14 December. The PCB stayed around  $65^\circ$  MLAT during the TOI, which is approximately  $10^\circ$  equatorward of its normal position.

[63] 6. The extreme expansion of the PCB was completed 1–1.5 h before the onset of the TOI and the boundary returned to higher latitudes when the TOI disappeared, suggesting that the “expansion of the high-latitude convection system” was one of the necessary conditions for the formation of the transpolar TOI.

[64] 7. An ionospheric positive storm occurred on the dayside at 2320 UT on 14 December and continued for about 4 h until 0340 UT on 15 December. Total electron content (TEC) increased to 40 TECU in the midlatitudes which could make the source plasma sufficiently dense for the generation of the bright TOI.

[65] 8. The enhancement of the source plasma occurred 1–1.5 h before the appearance of the TOI in the polar cap area and ceased 1–1.5 h before the disappearance of the TOI. This implies that the “build up of the source plasma in the midlatitudes” was another necessary condition for the formation of the TOI.

[66] 9. The above mentioned two necessary conditions for generating TOIs were satisfied almost simultaneously because both of them were caused by the prolonged large-amplitude IMF  $B_z$  starting at 2230 UT on 14 December. This allowed the TOI to be formed very promptly. That is, the prolonged large-amplitude southward IMF  $B_z$  in the later part of CME-driven storm could be the most important factor for producing large-scale transpolar TOI.

[67] 10. After the appearance at around 0140 UT, the TOI moved back and forth in the dawn to dusk direction very dynamically (Figure 24d). In particular, the TOI suddenly started moving downward at around 0250 UT and shifted its location for approximately 1000 km in some 15 min.

[68] 11. The IMF  $B_y$  and  $B_z$  were stable throughout the interval of the TOI, implying that the streamline of the polar cap convection did not change very much at the time of the dawnward excursion of the TOI. Hence, the change in IMF is unlikely to contribute to the rapid motion of the TOI in the central polar cap.

[69] 12. The SuperDARN radars observed a burst of westward flow on closed field lines about 1 h before the dawnward excursion of the TOI (Figures 24g and 24h). This flow was possibly responsible for transporting high-density plasma from the midlatitude to the cusp inflow region as an enhanced storm density (SED).

[70] 13. The SuperDARN data also show that the flow on closed field line progressed westward very rapidly. Such a progression shifted the possible entry point of the SED plasma into the polar cap dawnward and finally led to the dawnward excursion of the TOI in the central polar cap.

[71] 14. During the westward progression of the flow on closed field line, the midlatitude trough seen in the GPS-TEC data penetrated deep into the dayside sunlit area, which was possibly associated with the sunward extension of a SAPS. Thus, the dawnward excursion of the TOI could be caused by the temporal evolution of the SAPS on closed field lines.

[72] 15. There exist some differences between patches and TOIs in terms of their spatial structure. In particular, the optical signature of the TOI was found to be a continuous narrow stream elongated in the noon-midnight direction, while patches are normally observed as individual regions of airglow enhancement.

[73] 16. TOIs are generally broken into patches by IMF-driven large-scale temporal changes in the cusp plasma flow. However, the IMF was stable during this TOI, which allowed the SED entering the cusp to survive without being broken into discrete patches by the time-varying convection. This means that a very stable IMF in the later part of a CME-driven storm could be a necessary factor for maintaining the TOI continuous without being broken into patches.

[74] 17. There existed some mesoscale patterns embedded within the main body of the plume. The SuperDARN data (Figures 24g and 24h) show the existence of some smaller-scale temporal variations in the Doppler velocity both poleward and equatorward of the PCB. Such variation possibly modulated the spatial structure of TOI and finally contributed to the formation of the mesoscale structures within the TOI.

[75] In conclusion, the signature of polar cap TOI as visualized with the all-sky airglow imager was found to be much more dynamic and much more complicated than we ever thought, which is presumably caused by temporal variations in the global-scale plasma circulation system including flow burst on closed field line (i.e. SAPS), extreme expansion of the polar cap area, and plasma density enhancement in the dayside low-latitude to midlatitude ionosphere. Therefore, the plasma environment in the polar cap ionosphere during large magnetic storms should be described on the basis of a global-scale point of view.

[76] **Acknowledgments.** This work was supported by Grants-in-Aid for Scientific Research (16403007, 19340141, 19403010, 20244080, and 20740282) from the Japan Society for the Promotion of Science (JSPS). This work was carried out by the joint research program of the Solar-Terrestrial Environment Laboratory (STEL), Nagoya University. This work was performed using the facilities of STEL, Nagoya University. The authors thank Y. Katoh, M. Satoh, and T. Katoh of STEL, Nagoya University, for kind support in airglow imaging observations. Special thanks are extended to staff of the Narwhal Arctic Service at Resolute Bay for kind and helpful support in operating the optical instrument. The optical observation at Resolute Bay was also supported by the NSF cooperative agreement ATM-0608577. This research was partially supported by Special Funds for Education and Research (Energy Transport Processes in Geospace, Solar-Terrestrial Environment Laboratory, Nagoya University) of the Ministry of Education, Culture, Sports, Science, and Technology of Japan. We are also thankful for the data of the SuperDARN King Salmon radar operated by the National Institute of Information and Communications Technology (NICT). The authors wish to thank N. Ness at the Bartol Research Institute for access to data from MFI and SWE instruments on board the ACE spacecraft. The provisional AE,  $D_{st}$  and SYM index were provided by World Data Center (WDC) for Geomagnetism, Kyoto. The DMSP particle detectors were designed by D. Hardy of AFRL, and data were obtained from JHU/APL. We thank D. Hardy, F. Rich, and P. Newell for its use. We are also indebted to the PIs of the various SuperDARN radars, without whose efforts this study would not have been possible. The GPS data used in this study were obtained via the ftp servers of CORS (<ftp://www.ngs.noaa.gov/cors/rinex/>), SOPAC (<ftp://gamer.ucsd.edu/pub/rinex/>), and IGS (<ftp://cddisa.gsfc.nasa.gov/pub/gps/data/daily/>). We acknowledge IGS,

UNAVCO, SCIGN and its sponsors, the W. M. Keck Foundation, NASA, NSF, USGS, and SCEC for providing GPS data. SOHO is a project of international cooperation between ESA and NASA. The OMNI-2 data were obtained from NASA/NSSDC. The GOES and POES satellite data were provided from NOAA/NGDC. A part of this work was done while K.H. was staying at Department of Physics, University of Oslo as a guest researcher. His research at University of Oslo was supported by a grant of the "Excellent Young Researcher Overseas Visit Program" from JSPS.

[77] Robert Lysak thanks John Foster and another reviewer for their assistance in evaluating this paper.

## References

- Anderson, D. N., J. Buchau, and R. A. Heelis (1988), Origin of density enhancements in the winter polar cap ionosphere, *Radio Sci.*, **23**, 513–519.
- Araki, T. (1994), A physical model of the geomagnetic sudden commencement, in *Solar Wind Sources of Magnetospheric Ultra-Low-Frequency Waves*, *Geophys. Monogr. Ser.*, vol. 81, edited by M. Engebretson, K. Takahashi, and M. Scholer, pp. 183–200, AGU, Washington, D. C.
- Baker, K. B., and S. Wing (1989), A new magnetic coordinate system for conjugate studies of high latitudes, *J. Geophys. Res.*, **94**, 9139–9143.
- Barbier, D. (1959), Recherches sur la raie 6300 de la luminescence atmosphérique nocturne, *Ann. Geophys.*, **15**, 179–217.
- Barbier, D., and J. Glaume (1962), La couche ionosphérique nocturne *F* dans la zone intertropicale et ses relations avec l'émission de la raie 6300 Å du ciel nocturne, *Planet. Space Sci.*, **9**, 133–148.
- Basu, S., S. Basu, J. J. Makela, E. MacKenzie, P. Doherty, J. W. Wright, F. Rich, M. J. Keskinen, R. E. Sheehan, and A. J. Coster (2008), Large magnetic storm-induced nighttime ionospheric flows at midlatitudes and their impacts on GPS-based navigation systems, *J. Geophys. Res.*, **113**, A00A06, doi:10.1029/2008JA013076. [Printed 114(A3), 2009.]
- Burlaga, L., R. Skoug, C. Smith, D. Webb, T. Zurbuchen, and A. Reinard (2001), Fast ejecta during the ascending phase of solar cycle 23: ACE observations, 1998–1999, *J. Geophys. Res.*, **106**, 20,957–20,977, doi:10.1029/2000JA000214.
- Bust, G. S., and G. Crowley (2007), Tracking of polar cap ionospheric patches using data assimilation, *J. Geophys. Res.*, **112**, A05307, doi:10.1029/2005JA011597.
- Bust, G. S., and C. N. Mitchell (2008), History, current state, and future directions of ionospheric imaging, *Rev. Geophys.*, **46**, RG1003, doi:10.1029/2006RG000212.
- Carlson, H. C., Jr., K. Oksavik, J. Moen, and T. Pedersen (2004), Ionospheric patch formation: Direct measurements of the origin of a polar cap patch, *Geophys. Res. Lett.*, **31**, L08806, doi:10.1029/2003GL018166.
- Carlson, H. C., J. Moen, K. Oksavik, C. P. Nielsen, I. W. McCrea, T. R. Pedersen, and P. Gallop (2006), Direct observations of injection events of subauroral plasma into the polar cap, *Geophys. Res. Lett.*, **33**, L05103, doi:10.1029/2005GL025230.
- Chisham, G., et al. (2007), A decade of the Super Dual Auroral Radar Network (SuperDARN): Scientific achievements, new techniques and future directions, *Surv. Geophys.*, **28**, 33–109, doi:10.1007/s10712-007-9017-8.
- Chiu, M. C., et al. (1998), ACE spacecraft, *Space Sci. Rev.*, **86**, 257–284.
- Coley, W. R., and R. A. Heelis (1995), Adaptive identification and characterization of polar ionization patches, *J. Geophys. Res.*, **100**, 23,819–23,827.
- Crowley, G. (1996), Critical review of ionospheric patches and blobs, in *Review of Radio Science 1993–1996*, edited by W. R. Stone, p. 619–648, Oxford Univ. Press, New York.
- Decker, D., C. Valladares, R. Sheehan, S. Basu, D. Anderson, and R. Heelis (1994), Modeling daytime *F* layer patches over Sondrestrom, *Radio Sci.*, **29**, 249–268.
- De Franceschi, G., L. Alfonsi, V. Romano, M. Aquino, A. Dodson, C. N. Mitchell, P. Spencer, and A. W. Wernik (2008), Dynamics of high-latitude patches and associated small-scale irregularities during the October and November 2003 storms, *J. Atmos. Solar Terr. Phys.*, **70**, 879–888, doi:10.1016/j.jastp.2007.05.018.
- Ebihara, Y., N. Nishitani, T. Kikuchi, T. Ogawa, K. Hosokawa, and M. -C. Fok (2008), Two-dimensional observations of overshielding during a magnetic storm by the Super Dual Auroral Radar Network (SuperDARN) Hokkaido radar, *J. Geophys. Res.*, **113**, A01213, doi:10.1029/2007JA012641.
- Ebihara, Y., N. Nishitani, T. Kikuchi, T. Ogawa, K. Hosokawa, M.-C. Fok, and M. F. Thomsen (2009), Dynamical property of storm time subauroral rapid flows as a manifestation of complex structures of the plasma pressure in the inner magnetosphere, *J. Geophys. Res.*, **114**, A01306, doi:10.1029/2008JA013614.
- Evans, D. S., and M. S. Greer (2000), Polar orbiting environmental satellite space environment monitor - 2: Instrument descriptions and archive data documentation, *Tech. Memo. OAR SEC-93*, Natl. Oceanogr. Atmos. Admin., Boulder, Colo.
- Feldsten, Y. I., and G. V. Starkov (1967), Dynamics of auroral belt and polar geomagnetic disturbance, *Planet. Space Sci.*, **15**, 209–229.
- Foster, J. C. (1984), Ionospheric signatures of magnetospheric convection, *J. Geophys. Res.*, **89**, 855–865.
- Foster, J. C. (1989), Plasma transport through the dayside cleft: A source of ionization patches in the polar cap, in *Electromagnetic Coupling in the Polar Clefts and Caps*, edited by P. Sandholt and A. Egeland, p. 343–354, Kluwer Acad., Norwell, Mass.
- Foster, J. C. (1993), Storm-time plasma transport at middle and high latitudes, *J. Geophys. Res.*, **98**, 1675–1689.
- Foster, J. C. (2008), Ionospheric-magnetospheric-heliospheric coupling: Stormtime thermal plasma redistribution, in *Midlatitude Ionospheric Dynamics and Disturbances*, *Geophys. Monogr. Ser.*, vol. 181, edited by P. M. Kitner Jr. et al., pp. 121–134, AGU, Washington, D. C.
- Foster, J. C., and W. J. Burke (2002), SAPS: A new characterization for sub-auroral electric fields, *Eos Trans. AGU*, **83**(36), 393, doi:10.1029/2002EO000289.
- Foster, J. C., and J. R. Doupnik (1984), Plasma convection in the vicinity of the dayside cleft, *J. Geophys. Res.*, **89**, 9107–9113.
- Foster, J. C., and H. B. Vo (2002), Average characteristics and activity dependence of the subauroral polarization stream, *J. Geophys. Res.*, **107**(A12), 1475, doi:10.1029/2002JA009409.
- Foster, J. C., J. M. Holt, J. D. Kelly, and V. B. Wickwar (1985), High-resolution observations of electric fields and F-region plasma parameters in the cleft ionosphere, in *The Polar Cusp*, edited by J. A. Holtet and A. Egeland, p. 349–364, D. Reidel, Dordrecht, Netherlands.
- Foster, J. C., P. J. Erickson, F. D. Lind, and W. Rideout (2004), Millstone Hill coherent-scatter radar observations of electric field variability in the sub-auroral polarization stream, *Geophys. Res. Lett.*, **31**, L21803, doi:10.1029/2004GL021271.
- Foster, J. C., et al. (2005), Multiradar observations of the polar tongue of ionization, *J. Geophys. Res.*, **110**, A09S31, doi:10.1029/2004JA010928.
- Foster, J. C., W. Rideout, B. Sandel, W. T. Forrester, and F. J. Rich (2007), On the relationship of SAPS to storm-enhanced density, *J. Atmos. Solar Terr. Phys.*, **69**, 303–313, doi:10.1016/j.jastp.2006.07.021.
- Greenwald, R. A., et al. (1995), DARN/SuperDARN: A global view of the dynamics of high-latitude convection, *Space Sci. Rev.*, **71**, 761–796.
- Hardy, D. A., L. K. Schmitt, M. S. Gussenhoven, F. J. Marshall, H. C. Yeh, T. L. Schumaker, A. Huber, and J. Pantazis (1984), Precipitating electron and ion detectors (SSJ/4) for the block 5D/Flights 6–10 DMSP satellites: Calibration and data presentation, *Rep. AFGL-TR-84-0317*, Air Force Geophys. Lab., Hanscom Air Force Base, Lincoln, Mass.
- Hayashi, H., N. Nishitani, T. Ogawa, Y. Otsuka, T. Tsugawa, K. Hosokawa, and A. Saito (2010), Large-scale traveling ionospheric disturbance observed by superDARN Hokkaido HF radar and GPS networks on 15 December 2006, *J. Geophys. Res.*, **115**, A06309, doi:10.1029/2009JA014297.
- Hosokawa, K., T. Iyemori, A. S. Yukimatu, and N. Sato (2001), Source of field-aligned irregularities in the subauroral *F* region as observed by SuperDARN radars, *J. Geophys. Res.*, **106**, 24,713–24,731, doi:10.1029/2001JA900080.
- Hosokawa, K., M. Sugino, M. Lester, N. Sato, A. S. Yukimatu, and T. Iyemori (2002), Simultaneous measurement of duskside subauroral irregularities from the CUTLASS Finland radar and EISCAT UHF system, *J. Geophys. Res.*, **107**(A12), 1457, doi:10.1029/2002JA009416.
- Hosokawa, K., E. E. Woodfield, M. Lester, S. E. Milan, N. Sato, A. S. Yukimatu, and T. Iyemori (2003), Interhemispheric comparison of spectral width boundary as observed by the SuperDARN radars, *Ann. Geophys.*, **21**, 1553–1565, doi:10.5194/angeo-21-1553-2003.
- Hosokawa, K., K. Shiokawa, Y. Otsuka, A. Nakajima, T. Ogawa, and J. D. Kelly (2006), Estimating drift velocity of polar cap patches with all-sky airglow imager at Resolute Bay, Canada, *Geophys. Res. Lett.*, **33**, L15111, doi:10.1029/2006GL026916.
- Hosokawa, K., K. Shiokawa, Y. Otsuka, T. Ogawa, J.-P. St-Maurice, G. J. Sofko, and D. A. Andre (2009a), The relationship between polar cap patches and field-aligned irregularities as observed with an all-sky airglow imager at Resolute Bay and the PolarDARN radar at Rankin Inlet, *J. Geophys. Res.*, **114**, A03306, doi:10.1029/2008JA013707.
- Hosokawa, K., T. Kashimoto, S. Suzuki, K. Shiokawa, Y. Otsuka, and T. Ogawa (2009b), Motion of polar cap patches: A statistical study with all-sky airglow imager at Resolute Bay, Canada, *J. Geophys. Res.*, **114**, A04318, doi:10.1029/2008JA014020.
- Hosokawa, K., T. Tsugawa, K. Shiokawa, Y. Otsuka, T. Ogawa, and M. Hairston (2009c), Unusually elongated, bright airglow plume in the polar cap *F* region: Is it tongue of ionization?, *Geophys. Res. Lett.*, **36**, L07103, doi:10.1029/2009GL037512.
- Hosokawa, K., J. P. St-Maurice, G. J. Sofko, K. Shiokawa, Y. Otsuka, and T. Ogawa (2010), Reorganization of polar cap patches through shears in

- the background plasma convection, *J. Geophys. Res.*, *115*, A01303, doi:10.1029/2009JA014599.
- Ishida, T., K. Hosokawa, T. Shibata, S. Suzuki, N. Nishitani, and T. Ogawa (2008), SuperDARN observations of daytime MSTIDs in the auroral and mid-latitudes: Possibility of long-distance propagation, *Geophys. Res. Lett.*, *35*, L13102, doi:10.1029/2008GL034623.
- Iyemori, T., and D. R. K. Rao (1996), Decay of the Dst component of geomagnetic disturbance after substorm onset and its implication to storm substorm relation, *Ann. Geophys.*, *14*, 608–618.
- Jayachandran, P. T., K. Hosokawa, J. W. MacDougall, S. Mushini, R. B. Langley, and K. Shiokawa (2009), GPS total electron content variations associated with a polar cap arc, *J. Geophys. Res.*, *114*, A12304, doi:10.1029/2009JA014916.
- Kataoka, R., and Y. Miyoshi (2006), Flux enhancement of radiation belt electrons during geomagnetic storms driven by coronal mass ejections and corotating interaction regions, *Space Weather*, *4*, S09004, doi:10.1029/2005SW000211.
- Kataoka, R., S. Watari, N. Shimada, H. Shimazu, and K. Marubashi (2005), Downstream structures of interplanetary fast shocks associated with coronal mass ejections, *Geophys. Res. Lett.*, *32*, L12103, doi:10.1029/2005GL022777.
- Kataoka, R., N. Nishitani, Y. Ebihara, K. Hosokawa, T. Ogawa, T. Kikuchi, and Y. Miyoshi (2007), Dynamic variations of a convection flow reversal in the subauroral postmidnight sector as seen by the SuperDARN Hokkaido HF radar, *Geophys. Res. Lett.*, *34*, L21105, doi:10.1029/2007GL031552.
- Kataoka, R., T. Ebisuzaki, K. Kusano, D. Shiota, S. Inoue, T. T. Yamamoto, and M. Tokumaru (2009), Three-dimensional MHD modeling of the solar wind structures associated with 13 December 2006 coronal mass ejection, *J. Geophys. Res.*, *114*, A10102, doi:10.1029/2009JA014167.
- Khan, H., and S. W. H. Cowley (1999), Observations of the response time of high-latitude ionospheric convection to variations in the interplanetary magnetic field using EISCAT and IMP-8 data, *Ann. Geophys.*, *17*, 1306–1335.
- Knudsen, W. C. (1974), Magnetospheric convection and the high-latitude  $F_2$  ionosphere, *J. Geophys. Res.*, *79*, 1046–1055.
- Koustov, A., K. Hosokawa, N. Nishitani, T. Ogawa, and K. Shiokawa (2008), Rankin Inlet PolarDARN radar observations of duskward moving Sun-aligned optical forms, *Ann. Geophys.*, *26*, 2711–2723, doi:10.5194/angeo-26-2711-2008.
- Lei, J., W. Wang, A. G. Burns, S. C. Solomon, A. D. Richmond, M. Wiltberger, L. P. Goncharenko, A. Coster, and B. W. Reinisch (2008a), Observations and simulations of the ionospheric and thermospheric response to the December 2006 geomagnetic storm: Initial phase, *J. Geophys. Res.*, *113*, A01314, doi:10.1029/2007JA012807.
- Lei, J., A. G. Burns, T. Tsugawa, W. Wang, S. C. Solomon, and M. Wiltberger (2008b), Observations and simulations of quasiperiodic ionospheric oscillations and large-scale traveling ionospheric disturbances during the December 2006 geomagnetic storm, *J. Geophys. Res.*, *113*, A06310, doi:10.1029/2008JA013090.
- Lockwood, M., and H. C. Carlson (1992), Production of polar cap electron density patches by transient magnetopause reconnection, *Geophys. Res. Lett.*, *19*, 1731–1734.
- MacDougall, J., and P. T. Jayachandran (2007), Polar patches: Auroral zone precipitation effects, *J. Geophys. Res.*, *112*, A05312, doi:10.1029/2006JA011930.
- McComas, D. J., S. J. Bame, P. Barker, W. C. Feldman, J. L. Phillips, P. Riley, and J. W. Griffiee (1998), Solar Wind Electron Proton Alpha Monitor (SWEPAM) for the Advanced Composition Explorer, *Space Sci. Rev.*, *86*, 563–612.
- Milan, S., M. Lester, S. Cowley, and M. Brittner (2000), Convection and auroral response to a southward turning of the IMF: Polar UVI, CUTLASS, and IMAGE signatures of transient magnetic flux transfer at the magnetopause, *J. Geophys. Res.*, *105*, 15,741–15,755.
- Milan, S. E., M. Lester, and T. K. Yeoman (2002), HF radar polar patch formation revisited: summer and winter variations in dayside plasma structuring, *Ann. Geophys.*, *20*, 487–499.
- Milan, S. E., M. Lester, S. W. H. Cowley, K. Oksavik, M. Brittner, R. A. Greenwald, G. Sofko, and J.-P. Villain (2003), Variations in polar cap area during two substorm cycles, *Ann. Geophys.*, *21*, 1121–1140.
- Mishin, E. V., J. C. Foster, A. P. Potekin, F. J. Rich, K. Schlegel, K. Yumoto, V. I. Taran, J. M. Ruohoniemi, and R. Friedel (2002), Global ULF disturbances during a stormtime substorm on 25 September 25 1998, *J. Geophys. Res.*, *107*(A12), 1486, doi:10.1029/2002JA009302.
- Mishin, E. V., W. J. Burke, C. Y. Huang, and F. J. Rich (2003), Electromagnetic wave structures within subauroral polarization streams, *J. Geophys. Res.*, *108*(A8), 1309, doi:10.1029/2002JA009793.
- Mitchell, C. N., L. Alfonsi, G. De Franceschi, M. Lester, V. Romano, and A. W. Wernik (2005), GPS TEC and scintillation measurements from the polar ionosphere during the October 2003 storm, *Geophys. Res. Lett.*, *32*, L2S03, doi:10.1029/2004GL021644.
- Moen, J., H. C. Carlson, K. Oksavik, C. P. Nielsen, S. E. Pryse, H. R. Middleton, I. W. McCre, and P. Gallop (2006), EISCAT observations of plasma patches at sub-auroral cusp latitudes, *Ann. Geophys.*, *24*, 2363–2374, doi:10.5194/angeo-24-2363-2006.
- Moen, J., X. C. Qiu, H. C. Carlson, R. Fujii, and I. W. McCre (2008), On the diurnal variability in F2-region plasma density above the EISCAT Svalbard radar, *Ann. Geophys.*, *26*, 2427–2433, doi:10.5194/angeo-26-2427-2008.
- Moffett, R. J., and S. Quegan (1983), The mid-latitude trough in the electron concentration of the ionospheric F-layer: A review of observations and modelling, *J. Atmos. Terr. Phys.*, *45*, 315–343.
- Ogawa, T., S. Buchert, N. Nishitani, N. Sato, and M. Lester (2001), Plasma density suppression process around the cusp revealed by simultaneous CUTLASS and EISCAT Svalbard radar observations, *J. Geophys. Res.*, *106*, 5551–5564, doi:10.1029/2000JA900111.
- Ogawa, T., N. Nishitani, Y. Otsuka, K. Shiokawa, T. Tsugawa and K. Hosokawa (2009), Medium-scale traveling ionospheric disturbances observed with the SuperDARN Hokkaido radar, all-sky imager and GPS network, and their relation to concurrent sporadic E layer irregularities, *J. Geophys. Res.*, *114*, A03316, doi:10.1029/2008JA013893.
- Otsuka, Y., T. Ogawa, A. Saito, T. Tsugawa, S. Fukao, and S. Miyazaki (2002), A new technique for mapping of total electron content using GPS network in Japan, *Earth Planets Space*, *54*, 63–70.
- Otsuka, Y., K. Shiokawa, T. Ogawa, and P. Wilkinson (2004a), Geomagnetic conjugate observations of medium-scale traveling ionospheric disturbances at midlatitude using all-sky airglow imagers, *Geophys. Res. Lett.*, *31*, L15803, doi:10.1029/2004GL020262.
- Otsuka, Y., K. Shiokawa, T. Ogawa, T. Yokoyama, M. Yamamoto, and S. Fukao (2004b), Spatial relationship of equatorial plasma bubbles and field-aligned irregularities observed with an all-sky airglow imager and the Equatorial Atmosphere Radar, *Geophys. Res. Lett.*, *31*, L20802, doi:10.1029/2004GL020869.
- Pedatella, N. M., J. Lei, K. M. Larson, and J. M. Forbes (2009), Observations of the ionospheric response to the 15 December 2006 geomagnetic storm: Long-duration positive storm effect, *J. Geophys. Res.*, *114*, A12313, doi:10.1029/2009JA014568.
- Pokhotelov, D., C. N. Mitchell, P. S. J. Spencer, M. R. Hairston, and R. A. Heelis (2008), Ionospheric storm time dynamics as seen by GPS tomography and in situ spacecraft observations, *J. Geophys. Res.*, *113*, A00A16, doi:10.1029/2008JA013109.
- Pröls, G. W. (1995), Ionospheric F-region storms, in *Handbook of Atmospheric Electrodynamics*, vol. 2, edited by H. Volland, pp. 195–248, CRC Press, Boca Raton, Fla.
- Rees, M. H. (1963), Auroral ionisation and excitation by incident energetic electrons, *Planet. Space Sci.*, *11*, 1209–1218.
- Rich, F. J., and M. Hairston (1994), Large-scale convection patterns observed by DMSP, *J. Geophys. Res.*, *99*, 3827–3844.
- Rodger, A. S., R. J. Moffett, and S. Quegan (1992), The role of ion drift in the formation of the ionisation troughs in the mid- and high-latitude ionosphere - a review, *J. Atmos. Terr. Phys.*, *54*, 1–30.
- Rodger, A. S., M. Pinnock, J. R. Dudeney, K. B. Baker, and R. A. Greenwald (1994), A new mechanism for polar patch formation, *J. Geophys. Res.*, *99*, 6425–6436.
- Ruohoniemi, J., and K. Baker (1998), Large-scale imaging of high-latitude convection with Super Dual Auroral Radar Network HF radar observations, *J. Geophys. Res.*, *103*, 20,797–20,811.
- Ruohoniemi, J. M., and R. A. Greenwald (2005), Dependencies of high-latitude plasma convection: Consideration of interplanetary magnetic field, seasonal, and universal time factors in statistical patterns, *J. Geophys. Res.*, *110*, A09204, doi:10.1029/2004JA010815.
- Russell, C. T., and R. C. Elphic (1978), Initial ISEE magnetometer results: Magnetopause observations, *Space Sci. Rev.*, *22*, 681–715.
- Sato, T. (1959), Morphology of ionospheric F2 disturbances in the polar regions, A linkage between polar patches and plasmaspheric drainage plumes, *Rep. Ionos. Res. Space Res. Jpn.*, *131*, 91.
- Sato, T., and G. Rourke (1964), F-region enhancements in the Antarctic, *J. Geophys. Res.*, *69*, 4591–4607.
- Streltsov, A. V., and J. C. Foster (2004), Electrodynamic coupling in the magnetosphere-ionosphere coupling in the nightside subauroral zone, *Phys. Plasmas*, *11*, 1260, doi:10.1063/1.1647139.
- Shiokawa, K., Y. Katoh, M. Satoh, M. K. Ejiri, T. Ogawa, T. Nakamura, T. Tsuda, and R. H. Wiens (1999), Development of optical mesosphere thermosphere imagers (OMTI), *Earth Planets Space*, *51*, 887–896.
- Shiokawa, K., Y. Katoh, M. Satoh, M. K. Ejiri, and T. Ogawa (2000), Integrating-sphere calibration of all-sky cameras for nightglow measurements, *Adv. Space Res.*, *26*, 1025–1028.

- Shiokawa, K., C. Ihara, Y. Otsuka, and T. Ogawa (2003a), Statistical study of nighttime medium-scale traveling ionospheric disturbances using mid-latitude airglow images, *J. Geophys. Res.*, *108*(A1), 1052, doi:10.1029/2002JA009491.
- Shiokawa, K., et al. (2003b), Thermospheric wind during a storm-time large-scale traveling ionospheric disturbance, *J. Geophys. Res.*, *108*(A12), 1423, doi:10.1029/2003JA010001.
- Shiokawa, K., T. Ogawa, and Y. Kamide (2005), Low-latitude auroras observed in Japan: 1999–2004, *J. Geophys. Res.*, *110*, A05202, doi:10.1029/2004JA010706.
- Shiokawa, K., Y. Otsuka, and T. Ogawa (2009), Propagation characteristics of nighttime mesospheric and thermospheric waves observed by optical mesosphere thermosphere imagers at middle and low latitudes, *Earth Planets Space*, *61*, 479–491.
- Siscoe, G. L., and T. S. Huang (1985), Polar cap inflation and deflation, *J. Geophys. Res.*, *90*, 543–547.
- Smith, C. W., J. L'Heureux, N. F. Ness, M. H. Acuna, L. F. Burlaga, and J. Scheifele (1998), The ACE magnetic fields experiment, *Space Sci. Rev.*, *86*, 613–632.
- Stolle, C., J. Liliensten, S. Schluter, Ch. Jacobi, M. Rietveld, and H. Luhr (2006), Observing the north polar ionosphere on 30 October 2003 by GPS imaging and IS radars, *Ann. Geophys.*, *24*, 107–113, doi:10.5194/angeo-24-107-2006.
- Suzuki, S., K. Shiokawa, K. Hosokawa, K. Nakamura, and W. K. Hocking (2009a), Statistical characteristics of polar cap mesospheric gravity waves observed by an all-sky airglow imager at Resolute Bay, Canada, *J. Geophys. Res.*, *114*, A01311, doi:10.1029/2008JA013652.
- Suzuki, S., K. Hosokawa, T. F. Shibata, K. Shiokawa, Y. Otsuka, N. Nishitani, T. Ogawa, A. V. Koustov, and B. M. Shevtsov (2009b), Coordinated observations of nighttime medium-scale traveling ionospheric disturbances in 630-nm airglow and HF radar echoes at midlatitudes, *J. Geophys. Res.*, *114*, A07312, doi:10.1029/2008JA013963.
- Tsunoda, R. T. (1988), High latitude *F* region irregularities: A review and synthesis, *Rev. Geophys.*, *26*, 719–760.
- Valladares, C., S. Basu, J. Buchau, and E. Friis-Christensen (1994), Experimental evidence for the formation and entry of patches into the polar cap, *Radio Sci.*, *29*, 167–194.
- Weimer, D. R. (2005), Improved ionospheric electrodynamic models and application to calculating Joule heating rates, *J. Geophys. Res.*, *110*, A05306, doi:10.1029/2004JA010884.
- Wild, J. A., et al. (2003), Coordinated interhemispheric SuperDARN radar observations of the ionospheric response to flux transfer events observed by the Cluster spacecraft at the high-latitude magnetopause, *Ann. Geophys.*, *21*, 1807–1826.
- Yin, P., C. N. Mitchell, P. Spencer, I. McCreia, and T. Pedersen (2008), A multi-diagnostic approach to understanding high-latitude plasma transport during the Halloween 2003 storm, *Ann. Geophys.*, *26*, 2739–2747, doi:10.5194/angeo-26-2739-2008.

M. R. Hairston, William B. Hanson Center for Space Sciences, University of Texas at Dallas, P. O. Box 830688 WT15, Richardson, TX 75083-0688, USA. (hairston@utdallas.edu)

K. Hosokawa, Department of Communication Engineering and Informatics, University of Electro-Communications, Chofugaoka 1-5-1, Chofu, Tokyo 182-8585, Japan. (hosokawa@ice.uec.ac.jp)

N. Nishitani, Y. Otsuka, and K. Shiokawa, Solar-Terrestrial Environment Laboratory, Nagoya University, Furo-cho, Chikusa-ku, Nagoya 464-8601, Japan. (nisitani@stelab.nagoya-u.ac.jp; otsuka@stelab.nagoya-u.ac.jp; shiokawa@stelab.nagoya-u.ac.jp)

T. Ogawa and T. Tsugawa, National Institute of Information and Communications Technology, Nukui-Kitamachi 4-2-1, Koganei, Tokyo 184-8795, Japan. (taogawa@nict.go.jp; tsugawa@nict.go.jp)